Modeling Nucleobase Radicals in the Gas Phase. Experimental and Computational Study of 2-Hydroxypyridinium and 2-(1H)Pyridone Radicals

Jill K. Wolken and František Turecek*

Department of Chemistry, Bagley Hall, Box 351700, University of Washington, Seattle, Washington 98195-1700

Received: March 29, 1999; In Final Form: May 25, 1999

Isomeric radicals corresponding to hydrogen atom adducts to 2-hydroxypyridine (**1**) and 2-(1H)pyridone (**2**) were investigated by neutralization-reionization mass spectrometry and combined ab initio and density functional theory calculations. Gas-phase protonation of **1** and **2** occurred preferentially at the nitrogen and oxygen atoms, respectively, to give a single 2-hydroxypyridinium ion $\mathbf{3}^+$. The calculated topical proton affinities in **1** were 922, 602, 777, 649, 786, 694, and 746 kJ mol^{-1} for the N-1, C-2, C-3, C-4, C-5, C-6, and OH positions, respectively. The topical proton affinities in **2** were 756, 824, 815, 692, and 930 kJ mol^{-1} for the N-1, C-3, C-5, C-6, and carbonyl oxygen positions, respectively. The 2-hydroxy-(1H)pyridinium radical (**3**$^\bullet$) was generated by collisional neutralization of ion $\mathbf{3}^+$ and found to be stable on a 4.67 μs time scale. Radical **3**$^\bullet$ dissociated by losses of the hydroxyl and amine hydrogen atoms and by ring cleavages. MP2 and B3LYP calculations with the 6-311G(2d,p) basis set established the 298 K relative energies of hydrogen atom adducts derived from **1** and **2** as 3-H-**2** (**11**$^\bullet$, most stable, 0) < 6-H-**2** (**14**$^\bullet$, +20) < 3H-**1** (**5**$^\bullet$,+37) < 4H-**2** (**12**$^\bullet$,+59) < 5H-**2** (**13**$^\bullet$,+60) < 5H-**1** (**7**$^\bullet$,+62) < **3**$^\bullet$ (+67) < 6H-**1** (**8**$^\bullet$,+76) < 4H-**1** (**6**$^\bullet$,+86) < 2H-**1** (**4**$^\bullet$,+107) < 1H-**2** (**10**$^\bullet$,+139 kJ mol^{-1}). Hydrogen atom adducts to C-2 in **2** and to the hydroxyl group in **1** were found to be unstable and dissociated by ring opening and loss of H, respectively. RRKM calculations on the effective QCISD(T)/6-311+G(2d,p) potential energy surface showed cleavages of the O−H and N−H bonds in **3**$^\bullet$ to be the lowest energy dissociations occurring in a 10:1 ratio. **1** was calculated to be 4.7 kJ mol^{-1} more stable than **2** in the gas phase at 0 K. Fitting the experimental and calculated isotope effects on dissociations of deuterium-labeled radicals yielded a distribution function for the internal energy in the ground electronic state of **3**$^\bullet$ formed by collisional electron transfer. The maximum of the internal energy distribution in ground-state **3**$^\bullet$ (129 kJ mol^{-1}) was found to be expressed accurately by a combination of the internal energy of the precursor ion and the Franck−Condon energy gained on vertical electron transfer. The three lowest excited electronic states in **3**$^\bullet$ were found by CIS/6-311G(2d,p) calculations to be outer states resulting from excitation of the unpaired electron in **3**$^\bullet$ or electron capture by $\mathbf{3}^+$. The energetics and radiative lifetimes of the outer excited states of **3**$^\bullet$ allowed interpretation of the highly endothermic ring-cleavage dissociations. The unimolecular chemistry of **3** can be explained by a bimodal energy distribution due to the formation of the ground and excited electronic states upon femtosecond collisional electron transfer.

Introduction

Tautomerism in heterocyclic compounds relevant to the nucleobases guanine, uracil, cytosine, and thymine has been studied extensively by experiment and theory.[1] Since the nucleobases are multifunctional molecules, simpler models have often been used to probe the properties of a particular structure motif.[1] In particular, the 2-hydroxypyridine-2-(1H)pyridone system has been studied extensively as a model for nucleobase tautomerism in the gas phase[2] and in solution[3] in both the ground and excited electronic states.[4] In addition to the effects on hydrogen bonding and Watson−Crick base pairing,[5] the tautomer relative stabilities and populations in mixtures also underlie the question of nucleobase reactivities in radical reactions and electron capture occurring in the process of DNA damage.[6] The products and intermediates of radical reactions involving nucleobases or heterocyclic model compounds have been studied in solution using several ingenious methods, as reviewed.[7] However, elucidation of the structure of transient radical intermediates and determination of their relative stabilities, reaction products, and kinetics remain a challenging task.

Previous reports from this laboratory have shown that simple heterocyclic radicals pyrrolium,[8] imidazolium,[8] pyridinium,[9] and pyrimidinium,[10] as well as substituted derivatives 2-aminopyrimidinium,[10] 4-aminopyrimidinium,[10] (uracil + H)$^\bullet$,[11] and (thymine + H)$^\bullet$,[11] can be generated specifically by femtosecond electron transfer in the gas phase[11] and analyzed by neutralization−reionization mass spectrometry (NRMS).[12] The general strategy for the preparation of heterocyclic radicals of the (M + H)$^\bullet$ type, where M is the heterocycle molecule, consists of protonation of M with a gas-phase acid of well-defined acidity, as shown for 2-hydroxypyridine (**1**) and 2-(1H)pyridone (**2**) (Scheme 1). Protonation can be directed to the most basic site in the heterocycle or, by using gas-phase acids of gradually increasing acidities, less basic sites can also be targeted. The gas-phase cations $(M + H)^+$ are accelerated to >100 000 m s^{-1} velocities and discharged by a glancing collision with a polarizable electron donor such as trimethylamine or dimethyl disulfide.[13] Nondissociating radicals and their dissociation products are analyzed by mass spectrometry following collisional reionization. Reaction mechanisms for dissociations of

10.1021/jp991077g CCC: $18.00
Published on Web 07/20/1999

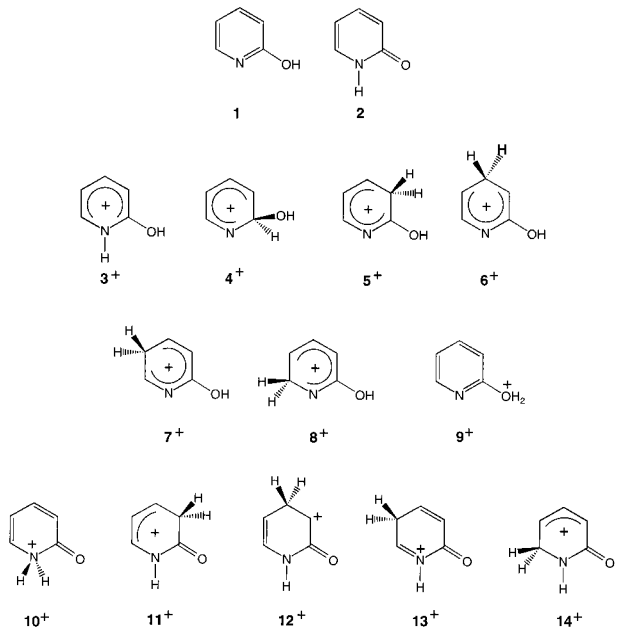

radical intermediates can usually be distinguished by isotope labeling or neutral collisional activation. In difficult cases, the neutral and post-reionization ion dissociations can be distinguished through their different temporal profiles using the method of variable-time NRMS.[14] Since NRMS data do not provide direct quantitative information on the radical energetics, ab initio and density functional theory calculations have been used to complement and interpret the experimental data.[8−11]

In a previous communication[15b] we have investigated the formations and dissociations of heterocyclic radicals derived from 3-hydroxypyridine, which exists as a single tautomer in the gas phase. In the present work we address the more complicated 2-hydroxypyridine (**1**)-2-(1H)-pyridone (**2**) system, which is known to consist of a ∼3:1 mixture of **1** and **2** in the gas phase.[16] The properties of the **1**/**2** tautomeric system have been studied previously by ab initio theory[2], semiempirical methods,[17] density-functional theory,[18] and matrix-isolation techniques[16c,d] and infrared,[19] Raman,[20] microwave,[21] UV−VIS,[22] fluorescence,[23] and photoionization spectroscopies[24] and mass spectrometry.[25] Pulse radiolysis,[26] radical oxidation,[27] and photochemical[28] studies of the **1**/**2** system have also been reported.

We use neutralization−reionization mass spectrometry in combination with deuterium labeling to elucidate the stabilities and dissociations of transient radicals corresponding to hydrogen atom adducts of **1** and **2**. Ab initio and density functional theory calculations are used to provide relative energies for cations and radicals and activation energies for radical dissociations and rearrangements. The activation energies were used for Rice−Ramsperger−Marcus−Kassel (RRKM) calculations of relative rate constants and determination of internal energy distribution in radicals formed by collisional electron transfer.

SCHEME 1

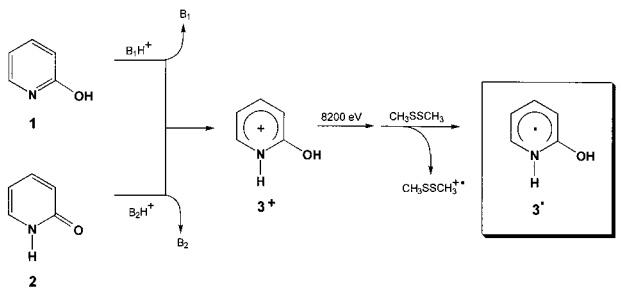

Experimental Section

Methods. Measurements were made on a tandem quadrupole acceleration−deceleration mass spectrometer as described previously.[29] Precursor cation radicals were generated by electron impact ionization (70 eV, 200 °C). Gas-phase protonation was achieved by ion−molecule reactions in a tight chemical-ionization ion source of our design.[29] CH_5^+/CH_4, H_3O^+/H_2O, $(CH_3)_2C{-}OH^+$/acetone, and NH_4^+/NH_3 were used as gas-phase acids for protonation. D_3O^+/D_2O and ND_4^+/ND_3 were used for deuteronation combined with H/D exchange of the acidic hydroxyl proton in the substrate molecule. CD_5^+/CD_4 and $(CD_3)_2C{-}OD^+$/acetone-d_6 were used for gas-phase deuteronations without OH/OD exchange. Stable precursor ions were extracted from the ion source, focused by an radio frequency-only quadrupole analyzer and accelerated to 8200 eV kinetic energy. The fast ions underwent neutralization by collisions with dimethyl disulfide at pressures allowing 70% transmittance of the precursor ion beam. The remaining ions were reflected by an electrostatic lens maintained at +250 V, and the neutral species were allowed to fly to a reionization chamber 60 cm downbeam. The lifetimes were 4.67, 4.70, and 4.72 μs for the $(M + H)^\bullet$, $(M + D)^\bullet$, and $(MD + D)^\bullet$ radicals at 8200 eV. The neutral products were reionized by collisions with oxygen (70% ion transmittance), the cations were decelerated, filtered by kinetic energy, and mass analyzed by a quadrupole mass analyzer operated at unit mass resolution. Collisional activation of the radical intermediates (NCR)[30] was performed by admitting helium to the lens system between the neutralization and reionization chambers. The helium pressure was adjusted to allow 70 or 50% transmittance of the precursor ion beam, and the lens potential was kept at +250 V to reject any ions formed in the lens. The reported spectra are averages of 30-40 consecutive scans taken at scan rate of 1 mass unit/s. The spectra were reproduced over the period of several weeks.

Collisionally activated dissociation (CAD) measurements were made on a JEOL HX-110 doubly focusing mass spectrometer of an EB geometry (electrostatic sector E precedes magnet B). Air was used as a collision gas at pressures allowing 50% transmittance of the ion beam at 10 keV. CAD were monitored in the first field-free region, and the spectra were recorded using a linked B/E scan. The spectra were averaged over 10−12 consecutive scans. CAD spectra using mass-analyzed kinetic energy scans (MIKES) were also measured on the Copenhagen four-sector JEOL HX-110/HX-110 mass spectrometer using oxygen as collision gas at 70% precursor ion beam transmittance. The precursor ion was selected by the first two sectors (EB) at mass resolution ∼3000.

Materials. 2-Hydroxypyridine (a mixture of **1** and **2**, Aldrich) was used as received and sampled into the ion source from a heated glass direct probe. Dimethyl disulfide (Aldrich) was purified by several freeze−pump−thaw cycles before use. 2-Hydroxypyridine-OD (**1-OD**) in mixture with 2-(1D)-pyridone (**2-ND**) was prepared by repeated H/D exchange in D_2O, the solvent was evaporated with a stream of dry nitrogen gas, and the product was stored in a desiccator under nitrogen.

Calculations. Standard ab initio calculations were performed by using the Gaussian 94 suite of programs.[31] Geometries were optimized with Hartree−Fock calculations using the 6-31G-(d,p) basis set. A spin-unrestricted formalism (UHF) was used for the radicals. The optimized structures were characterized by harmonic frequency analysis (all frequencies real). The

frequencies were corrected by 0.893[32] and used to calculate zero-point vibrational corrections and 298 K enthalpies. Complete optimized geometries (Cartesian coordinates) and uncorrected harmonic frequencies for all species are given as Supporting Information. Single-point energies were calculated with the Møller−Plesset perturbational theory[33] truncated at second order (MP2) using frozen core excitations. Contamination by higher spin states in UHF and UMP2 calculations was corrected in part by Schlegel's spin annihilation procedure.[34] Another set of single-point energies was calculated with density functional theory using Becke's three-parameter hybrid functional (B3LYP),[35] which incorporates a local correction functional of Vosko, Wilk, and Nusair[36] and a nonlocal density term according to Lee, Yang, and Parr.[37] Both sets of single-point calculations used the larger 6-311G(2d,p) basis set, which had been shown previously to provide reasonably accurate relative energies and proton affinities for several ionic and radical heterocyclic systems.[8−11,38] Additional calculations were also performed with the 6-311+G(2d,p) basis set for selected systems. Relative energies for radicals, transition states, and dissociation energies were obtained by averaging the spin-projected MP2 (PMP2) and B3LYP energies.[11,38] Another set of relative and activation energies were obtained by a composite procedure including quadratic configuration interaction,[39] QCISD(T)/6-31G(d,p), and PMP2/6-311+G(2d,p) calculations, according to eq 1.[38]

$$\text{QCISD(T)/6-311+G(2d,p)} \approx \text{QCISD(T)/6-31G(d,p)} + \text{PMP2/6-311+G(2d,p)} - \text{PMP2/6-31G(d,p)} \quad (1)$$

Effective QCISD(T)/6-311+G(2d,p) energies from eq 1 were insensitive to spin contamination in the UHF wave functions because the residual spin contamination in the projected MP2 energies canceled out to within 0.5 mhartree. RRKM calculations were performed using Hase's program[40] and direct counting of quantum states, as described previously.[15] Excited-state energies were calculated with the configuration interaction singles (CIS)[41] method using the 6-311G(2d,p) basis set.

Results and Discussion

Protonation of 2-Hydroxypyridine and 2-(1H)Pyridone. Precursor cations for the generation of transient radicals were produced by gas-phase protonation of 2-hydroxypyridine consisting of a mixture of **1** and **2**. The protonation exothermicities were defined by the proton affinities (PA) of **1** and **2** and those of the reagent conjugate bases,[42] methane (544 kJ mol^{-1}), water (690 kJ mol^{-1}), acetone (812 kJ mol^{-1}), and ammonia (854 kJ mol^{-1}) (eq 2).

$$-\Delta H_r = \text{PA}(\mathbf{1},\mathbf{2}) - \text{PA(reagent)} \quad (2)$$

Since only exothermic protonations are kinetically competitive in ion−molecule reactions in the gas phase,[43] the protonation regioselectivities were determined by the topical proton affinities of **1** and **2**. Interestingly, the proton affinity of **1**/**2** has not been determined experimentally;[44] an estimate from core electron binding energies[45] placed the gas-phase basicity of **1**/**2** close to that of pyridine (PA = 924 kJ mol^{-1}).[42] Here we assessed the topical PA in **1** and **2** by MP2 and B3LYP/6-311G(2d,p) calculations, as summarized in Table 1. The calculated PA values showed that the nitrogen atom in **1** (PA = 923 kJ mol^{-1}) and the carbonyl oxygen in **2** (PA = 930 kJ mol^{-1}) were the most basic sites. Previous DFT calculations bracketed the proton affinities of **1** and **2** between 916 and 963 kJ mol^{-1}.[46] The other positions in **1** and **2** were substantially less basic (Table 1). Protonation at C-4 in **2** did not result in a stable ion (**12**$^+$); instead, upon attempted geometry optimization structure **12**$^+$ rearranged to **11**$^+$ (Scheme 2). This result is not too surprising in view of **12**$^+$ being an α-oxocarbenium ion which can be expected to be substantially destabilized.[47]

TABLE 1: Topical Proton Affinities in 2-Hydroxypyridine and 2-(1H)Pyridone[a]

	2-hydroxypyridine		2-(1H)pyridone	
position	MP2[b]	B3LYP[b]	MP2	B3LYP
N-1	914	931	753	760
C-2	583	621		
C-3	759	795	815	833
C-4	631	667	*b*	*b*
C-5	769	803	809	820
C-6	674	714	675	710
O	744	748	927	933

[a] In units of kJ mol^{-1} at 298 K. Calculations with the 6-311G(2d,p) basis set and HF/6-31G(d,p) zero point and thermal corrections. [b] Unstable ion isomer.

SCHEME 2

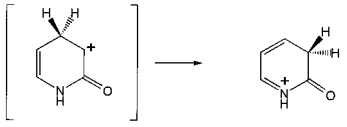

The calculated topical proton affinities were further used to predict the protonation sites in **1** and **2**. NH_4^+ must attack the most basic sites in **1** and **2** exclusively to produce the most stable ion isomer, **3**$^+$, from both **1** and **2** (Scheme 1). This convergent protonation thus obliterated the problem of dealing with the tautomeric mixture of **1** and **2**. Exothermic protonation with $(CH_3)_2C-OH^+$ was predicted to be completely regioselective in **1** to produce ion **3**$^+$. In **2**, protonation with $(CH_3)_2C-OH^+$ at oxygen should also predominate to yield **3**$^+$. In addition, protonations at C-3 and C-5 were marginally exothermic and could possibly result in formations of **11**$^+$ and **13**$^+$. These minor isomers could possibly contaminate the precursor ion beam. Since the formation of **11**$^+$ and **13**$^+$ was contingent upon the population of **2** in the gas phase, the composition of the **1**/**2** mixture at the ion source temperature was of interest.

The composition of the **1**/**2** mixture in the range of temperatures used for gas-phase protonations (200−250 °C) was assessed from ΔG_T values obtained by combined MP2 and B3LYP/6-311G(2d,p) and effective QCISD(T)/6-311+G(2d,p) relative energies and HF/6-31G(d,p) zero point corrections, enthalpies, and entropies. Both sets of calculations predicted **1**/**2** ratios >2. According to the higher level QCISD(T) calculations which gave $\Delta H_0(\mathbf{2}) - \Delta H_0(\mathbf{1}) = 4.7$ kJ mol^{-1} at 0 K, the fraction of **1** was 73−71% at 473−523 K. Hence, **1** should be the predominating isomer in the gas phase. These results were in very good general agreement with the few experimental determinations of **1**/**2** from gas-phase equilibria, which gave ratios ranging from 1.5 to 3.99 at different temperatures.[16] Most previous high-level theoretical calculations also predicted **1** to be the predominating isomer in the gas phase, although the calculated energy differences depended on the level of theory used.[2]

Since **2** was a minor component in the **1**/**2** mixture and protonation at C-3 and C-5 was less efficient than at oxygen, the contamination with **11**$^+$ and **13**$^+$ upon protonation with $(CH_3)_2C-OH^+$ should be negligible, and the precursor ion should consist mainly of **3**$^+$. On the basis of the energetics alone,

TABLE 2: Protonation Energies for 2-Hydroxypyridine and 2-(1H)Pyridone[a]

	$-\Delta H_{r,298}$[a,b]			
position	NH_4^+	$(CH_3)_2C{-}OH^+$	H_3O^+	CH_5^+
2-Hydroxypyridine				
N-1	69	110	232	378
C-2	*c*			58
C-3			87	233
C-4				105
C-5			96	242
C-6			4	150
O			56	202
2-(1H)Pyridone				
N-1				212
C-3		12	134	280
C-5		2	125	270
C-6			2	148
O	77	118	240	386

[a] From averaged MP2 and B3LYP topical proton affinities in kJ mol^{-1}. [b] Based on experimental proton affinities of ammonia (853.5 kJ mol^{-1}), acetone (812 kJ mol^{-1}), water (690 kJ mol^{-1}), and methane (544 kJ mol^{-1}). Data from ref 42. [c] Endothermic protonations (not shown).

SCHEME 3

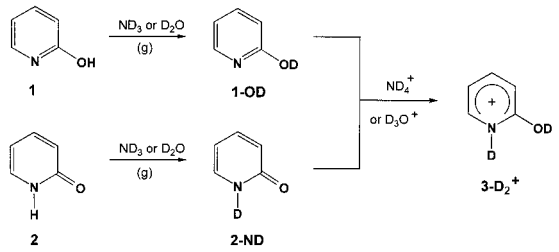

SCHEME 4

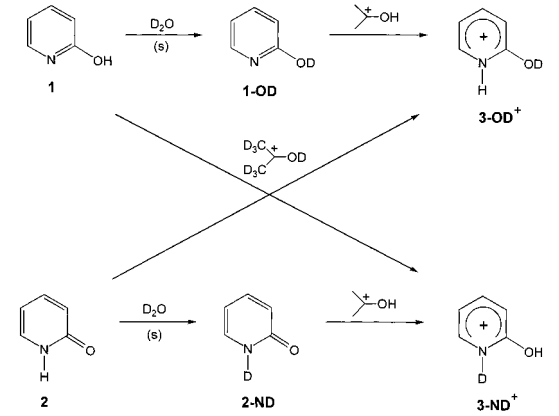

protonation with H_3O^+ could be less regioselective, and the strongest acid CH_5^+ could nominally attack any site in **1** and **2** (Table 2).

Deuterium labeling in the gas-phase ions was achieved in two ways. First, *exchanging* gas-phase acids, ND_4^+/ND_3 and D_3O^+/D_2O, were used to prepare **3-D$_2$**$^+$ by exchange of the acidic N−H and O−H protons in **1** and **2** for deuterium, followed by gas-phase deuteronation. This yielded a single isotopomer (**3-D$_2$**$^+$) from both **1** and **2** (Scheme 3). Second, partial labeling was accomplished by combination of solution H/D exchange of the acidic O−H and N−H protons and gas-phase protonation or deuteronations using *nonexchanging acids*, such as $(CD_3)_2C{-}OD^+$ or CD_5^+ (Scheme 4). In preparing the partially labeled ions, allowance must be made for the different protonation sites and positions of exchangeable protons or deuterons in the starting molecules **1** and **2**. For example, **1-OD**, in which the hydroxyl H was exchanged for D, formed the **3-OD**$^+$ ion following selective gas-phase protonation. Concurrently, the accompanying fraction of **2** exchanged the NH proton to give **2**-ND, which yielded **3-ND**$^+$ upon protonation in the gas phase. It was presumed that these isotopomeric ions were formed in a ratio which reflected the **1**/**2** ratio in the gas phase as discussed above. A different mixture with a reversed ratio of **3-OD**$^+$ and **3-ND**$^+$ was prepared by direct gas-phase deuteronation of **1** and **2**.

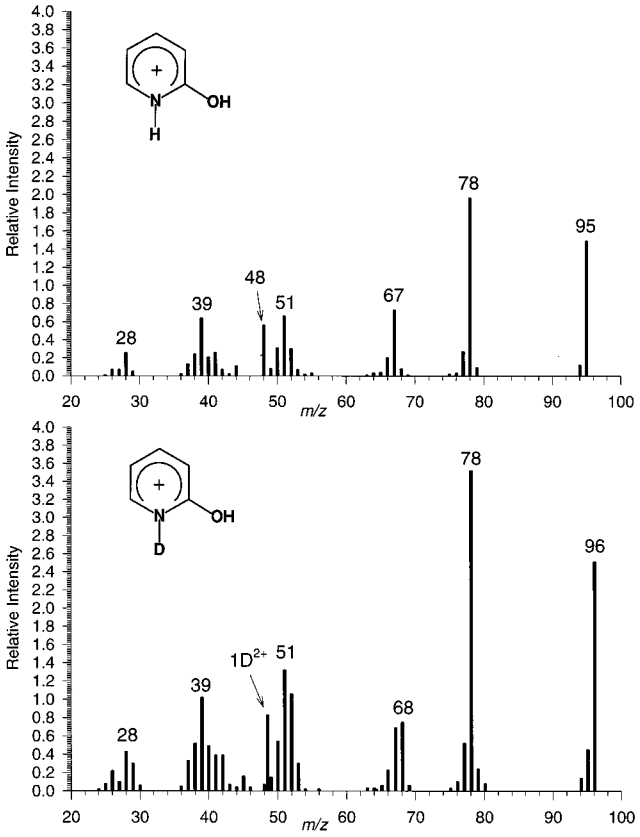

Figure 1. Collisionally activated dissociation (CAD) spectra of (a, top) **3**$^+$, (b, bottom) **3-OD**$^+$ and **1-ND**$^+$ from deuteronation with $(CD_3)_2C{-}OD^+$. Air as collision gas at 70% ion beam transmittance.

The gas-phase chemistry of **3**$^+$ and its isotopomers **3-D$_2$**$^+$, **3-ND**$^+$, and **3-OD**$^+$ was investigated through collisionally activated dissociation spectra (CAD, Figure 1). The major dissociations were loss of H, H_2O, COH, and ring cleavages forming the $C_4H_{2-4}^+/C_3H_{0-2}N^+$, $C_3H_{1-3}^+/C_2NH_{0-2}^+$, and $HC{-}NH^+$ ions. The loss of a hydrogen atom involved hydrogens from all positions, as revealed by deuterium labeling. For example, **3-D$_2$**$^+$ from deuteronation of (**1-OD** + **2-ND**) with $(CD_3)_2C{-}OD^+$ eliminated H and D in a 73:27 ratio, which was only slightly higher than the 67/33 ratio expected for a random loss of H or D from any position in **3-D$_2$**$^+$. CAD of **3-OD**$^+$ and **3-ND**$^+$ showed losses of H and D atoms in 83:17 and 85:15 ratios, respectively, to be compared with the 83:17 ratio for a purely statistical loss. These results clearly indicated that the loss of H from **3**$^+$ involved hydrogen atoms from all positions in **3**$^+$. Available thermochemical data allowed us to estimate the thresholds for the dissociations, **3**$^+ \rightarrow$ **1**$^{+\bullet}$ + H$^\bullet$ and **3**$^+ \rightarrow$ **2**$^{+\bullet}$ + H$^\bullet$ as 425 and 480 kJ mol^{-1}, respectively,[48] which were substantially higher than the typical energy barriers to proton migration in protonated aromatic ions (100−150 kJ mol^{-1}).[49] Extensive hydrogen scrambling in **3**$^+$ was therefore expected to precede loss of H in dissociating ions, as indeed observed.

In summary, the CAD measurements identified small neutral species that were formed by ion dissociations and that could

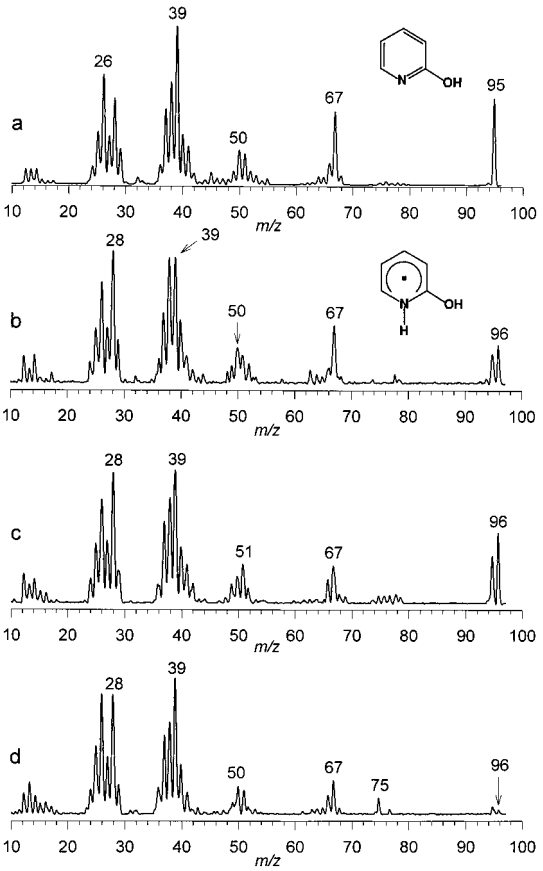

Figure 2. Neutralization (CH_3SSCH_3, 70% transmittance)−reionization (O_2, 70% transmittance) mass spectra of (a) $\mathbf{1}^{+\bullet}$ and $\mathbf{3}^+$ prepared by protonations with (b) NH_4^+, (c) H_3O^+, and (d) CH_5^+.

present interferences in the study of radical dissociations following collisional electron transfer.

Radical Formation and Dissociations. Collisional neutralization of $\mathbf{3}^+$ formed a fraction of radicals $\mathbf{3}^\bullet$ that gave rise to nondissociating (survivor) ions in the NRMS spectra (Figure 2b−d). This result established that $\mathbf{3}^\bullet$ were stable species on the time scale of the experiment (4.67 μs). The fractions of survivor ions, denoted as [**3**], depended on the internal energies of the precursor ions $\mathbf{3}^+$, which were in turn limited by the corresponding protonation exothermicities (eq 1, vide supra). $\mathbf{3}^+$ prepared by protonation with NH_4^+ (Figure 2b), $(CH_3)_2C-OH^+$, and H_3O^+ (Figure 2c) yielded [**3**] = 2.2−3.5% ΣI_{NR}, where ΣI_{NR} is the sum of all ion intensities in the NR mass spectrum. The most energetic $\mathbf{3}^+$ prepared by protonation with CH_5^+ yielded a substantially smaller fraction of survivor ions, [**3**] = 0.3% ΣI_{NR} (Figure 2d). The major dissociations of $\mathbf{3}^\bullet$ were loss of H (*m*/*z* 95), expulsion of COH to form pyrrole (*m*/*z* 67), and ring cleavages resulting in the formation of small fragments C_2H_2/CN (*m*/*z* 26), HCNH (*m*/*z* 28), and $C_3H_{0-3}/C_2H_{0-3}N$ (*m*/*z* 36−41) (Figure 2). Some of these dissociations also occurred on CAD of ions $\mathbf{3}^+$, although the product ion relative intensities in the CAD and NR spectra differed (cf. Figures 1 and 2).

Isotope effects on the stability of $\mathbf{3}^\bullet$ were observed for $\mathbf{3\text{-}D_2}^\bullet$ prepared by deuteronation with ND_4^+ and $(CD_3)_2C-OD^+$, [$\mathbf{3\text{-}D_2}$]/[**3**] = 1.46 and 3.1, respectively (Figures 3 and 4). In contrast, negligible isotope effects were observed for the relative abundances of [$\mathbf{3\text{-}D_2}$] in NR of ions prepared by deuteronation with D_3O^+ and CD_5^+ (spectra not shown). Deuterium labeling in $\mathbf{3\text{-}OD}^+$, $\mathbf{3\text{-}ND}^+$, and $\mathbf{3\text{-}D_2}^+$ allowed us to distinguish some reaction mechanisms specific to neutral dissociations. $\mathbf{3\text{-}D_2}^+$, prepared by gas-phase deuteronation−exchange with ND_4^+/ND_3

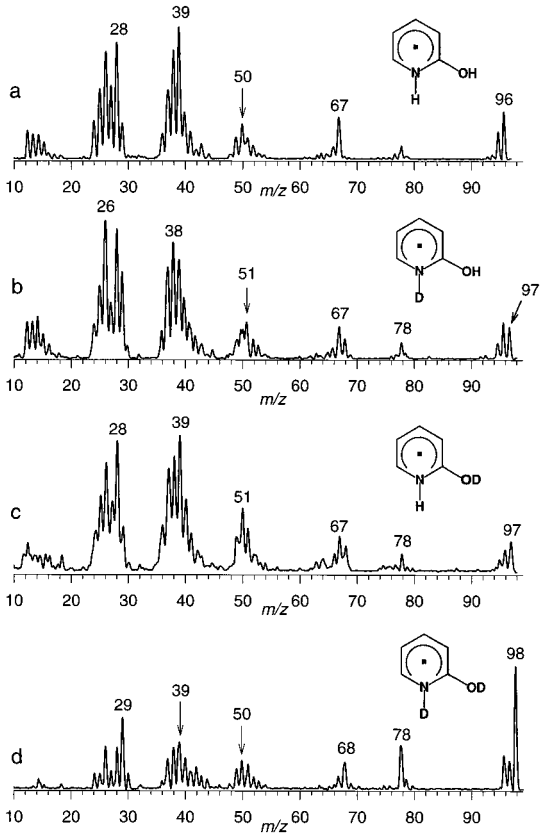

Figure 3. Neutralization (CH_3SSCH_3, 70% transmittance)−reionization (O_2, 70% transmittance) mass spectra of (a) $\mathbf{3}^+$, (b) $\mathbf{3\text{-}OD}^+$, (c) $\mathbf{3\text{-}ND}^+$, and (d) $\mathbf{3\text{-}D_2}^+$. The precursor ions were prepared by protonation with $(CH_3)_2C-OH^+$ and deuteronation with $(CD_3)_2C-OD^+$.

TABLE 3: Fractions of H and D Loss in the NR Mass Spectra

		%loss	
ion	preparation	H	D
$\mathbf{3\text{-}D_2}^+$	ND_3/ND_4^+	52	48
$\mathbf{3\text{-}D_2}^+$	$D_2O(s)/(CD_3)_2C-OD^+$	53	47
$\mathbf{3\text{-}D_2}^+$	D_2O/D_3O^+	7	93
$\mathbf{3\text{-}D_2}^+$	$D_2O(s)/CD_5^+$	50	50
$\mathbf{3\text{-}OD}^+ + \mathbf{3\text{-}ND}^+$	$D_2O(s)/(CH_3)_2C-OH^+$	68	32
$\mathbf{3\text{-}OD}^+ + \mathbf{3\text{-}ND}^+$	$D_2O(s)/CH_5^+$	54	46
$\mathbf{3\text{-}ND}^+ + \mathbf{3\text{-}OD}^+$	$(CD_3)_2C-OD^+$	63	37
$\mathbf{3\text{-}ND}^+ + \mathbf{3\text{-}OD}^+$	CD_5^+	54	46

showed loss of D and H in a 52:48 ratio (Table 3). This differed from the product distribution by ion dissociations which preferred loss of H. Collisional activation of radicals $\mathbf{3\text{-}D_2}^\bullet$ resulted in an increased overall dissociation and also an increased specificity for D loss (Figure 4a−c). When 30% of $\mathbf{3\text{-}D_2}^\bullet$ was allowed to undergo collisional activation, the loss of D and H occurred in a 69/31 ratio (Figure 4b), whereas on collisional activation of 50% $\mathbf{3\text{-}D_2}^\bullet$, the ratio further increased to 87:13 (Figure 4c). These results pointed to a highly regiospecific loss of H or D from the N−(H,D) and O−(H,D) positions in *neutral* $\mathbf{3}^\bullet$ and its isotopomers, as opposed to the random loss from ions $\mathbf{3}^+$ through $\mathbf{3\text{-}D_2}^+$.

An alternative explanation would presume that the intermediate radicals were energized by collisional activation, but the observed dissociations occurred after collisional reionization. Therefore, the effect on the H/D loss of increasing the number of collisions in the CAD spectra of $\mathbf{3\text{-}OD}^+$ was examined. At 70% ion beam transmittance, Poisson distribution predicted 83% single collisions while at 50% transmittance it was 69% single collisions. The fractions for H/D loss from $\mathbf{3\text{-}OD}^+$ did not

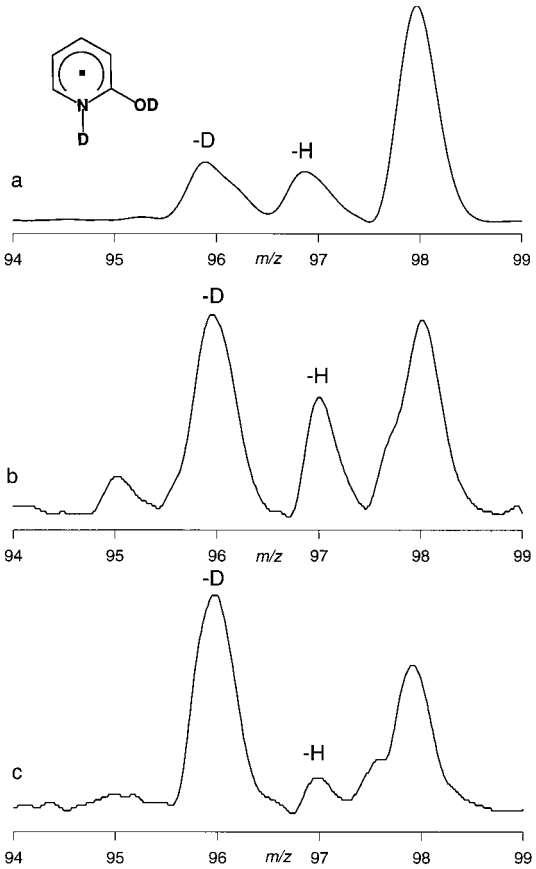

Figure 4. NR and NCR mass spectra of **3-D$_2$**$^+$ prepared by exchange−deuteronation with ND_3/ND_4^+. (a) NR spectrum, (b) NCR, He at 70% transmittance, (c) NCR He at 50% transmittance.

change beyond the experimental error (±2%). Hence CAD ion dissociations were insensitive to the mode of ion excitation. This result was in line with the energetics for the loss of H from **3**$^+$, which requires an estimated 425 and 480 kJ mol^{-1} to form **1**$^{+\bullet}$ and **2**$^{+\bullet}$, respectively, at the thermochemical threshold at 298 K.[48] Such high-energy dissociations are usually insensitive to variations of internal energy in the dissociating ion.[50] NR of **3-D$_2$**$^+$ prepared by $(CD_3)_2C{-}OD^+$ deuteronation of **1-OD**/**2-ND** showed a 47/53 ratio for loss of H/D, which did not differ substantially from that for **3-D$_2$**$^+$ prepared by the less exothermic deuteronation with ND_4^+ (vide supra). The loss of H can be attributed to nonspecific, post-reionization dissociations of **3-D$_2$**$^+$ similar to those discussed above. The relative abundances of products because of loss of H and D from **3-D$_2$**$^\bullet$ were fitted in the mass balance equation (eq 3), where D_{NRMS}, D_N, and D_i are the normalized fractions for loss of D from combined NR, neutral, and post-reionization ion dissociations,

$$D_{NRMS} = (1 - \alpha_N)D_i + \alpha_N D_N \qquad (3)$$

respectively, and α_N is the fractional contribution of the neutral dissociations. The value of $D_i = 0.27$ was taken from the CAD spectrum of **3-D$_2$**$^+$. The value of D_N was estimated as >0.9 based on the NCR spectrum of **3-D$_2$**, which showed mostly neutral dissociations. Under these assumptions, eq 3 predicted that upon NR the loss of H,D from **3-D$_2$** was composed of 28% neutral and 72% post-reionization ion dissociations for **3-D$_2$**$^+$ prepared by deuteronation/exchange with ND_4^+/ND_3. Very similar fractions (27% neutral and 73% post-reionization ion dissociations) were obtained for **3-D$_2$**$^+$ prepared by $(CD_3)_2C{-}OD^+$ deuteronation of a mixture **1**-OD and **2**-ND.

NR of the partially labeled ions **3-OD**$^+$ and **3-ND**$^+$ showed similar losses of H and D in approximately 2:1 ratios (Table 3). In this case a clear-cut distinction of the N−D and O−D bond cleavages could not be made, because the ion preparations in each case gave mixtures of **3-ND**$^+$ and **3-OD**$^+$ (vide supra), and the losses of H and D were affected by kinetic isotope effects as discussed below.

NR of **3-D$_2$**$^+$ from exchange−deuteronation with D_2O/D_3O^+ showed highly specific loss of D (93%). This result showed that isomers other than **3-D$_2$**$^+$ were not present in the ion beam, because deuteronation at C-3 through C-6 would have resulted in *increased* fractions for loss of H upon NR. Note that deuteronation with D_3O^+ could occur exothermically at C-3, C-5, and O in **1** and at N, C-3, and C-5 in **2**. The fact that C-3 and C-5 deuteronated ions were not present indicated that, if formed, they underwent exothermic D^+ transfer to the more basic N and O positions in neutral **1** and **2** in the ion source.

A yet different result was obtained for the most exothermic deuteronation with CD_5^+ (Table 3), which showed ∼50:50 ratios for H and D loss regardless of the mode of ion preparation. It should be noted that the exothermicity of protonation with CH_5 (or CD_5^+) was sufficient to cause extensive isomerization by H^+ or D^+ migrations in nondissociating ions. The energy barriers for such isomerizations can be estimated at <150 kJ mol^{-1},[49] which is less than the dissociation energy in **3**$^+$ and its isomers. Ion isomerization could occur during the flight time between the ion source and the neutralization cell (20−40 μs). Note that in this essentially collision-free region the less stable ion isomers would not be depleted efficiently by ion−molecule reactions.

In addition to loss of a hydrogen atom, NR also induced ring cleavages that gave rise to small fragments of the C_3H_{0-3}, $C_2H_{0-2}N$, C_2H_{0-2}, and $CH_{0-2}N$ groups (Figure 2). These fragments also appeared in the NR mass spectrum of **1,2** (Figure 2a). However, the relative abundance of survivor [**1** + **2**]$^{+\bullet}$ (5.2%ΣI_{NR}) from NR of the cation-radical was greater than the relative abundance of [**1** + **2**]$^{+\bullet}$ from NR of **3**$^+$ (0.6−3.3% ΣI_{NR}). This difference can arise if radical **3**$^\bullet$ underwent ring-cleavage dissociations or if **1** was formed from **3**$^\bullet$ with substantial internal energy that drove its molecular or post-reionization dissociations. Since the products of ring-cleavage dissociations in **3**$^\bullet$, **3**$^+$, and **1**$^{+\bullet}$ overlapped, the spectra alone did not permit distinction of these processes in the species involved. A deeper insight was therefore sought by investigating the dissociation energetics and kinetics by combined ab initio, DFT, and RRKM calculations.

Radical Energetics. Geometry optimizations yielded local energy minima for radicals **3**$^\bullet$− **8**$^\bullet$ derived from 2-hydroxypyridine **1** (Figure 5), **10**$^\bullet$−**15**$^\bullet$ derived from 2-(1H)pyridine (Figure 6), open-ring isomers, and transition states (Figure 7). The 2-pyridylhydroxonium radical (**9**$^\bullet$) dissociated to **1** and a hydrogen atom upon attempted geometry optimization. Radical **15**$^\bullet$ underwent ring opening by cleavage of the N−C-2 bond (Figure 6). The ordering of relative stabilities for radicals **3**$^\bullet$−**8**$^\bullet$ and **10**$^\bullet$−**15**$^\bullet$ (Table 4) differed from that for the corresponding cations (Table 1). According to the averaged PMP2 and B3LYP energies, **5**$^\bullet$ was the most stable structure among the radicals derived from **1**, followed by **7**$^\bullet$, **3**$^\bullet$, **8**$^\bullet$, **6**$^\bullet$, and **4**$^\bullet$. Radical **11**$^\bullet$ derived from **2** was the global minimum among the species studied.

The relative stabilities in the 2-pyridone series can be related to the electronic structure of the isomeric radicals as documented by the topical spin densities calculated for **11**$^\bullet$−**14**$^\bullet$ by UHF/6-311+G(2d,p) (Figure 8). The most stable isomer **11**$^\bullet$ was an allylic radical substituted by a weak electron-donating acylamino

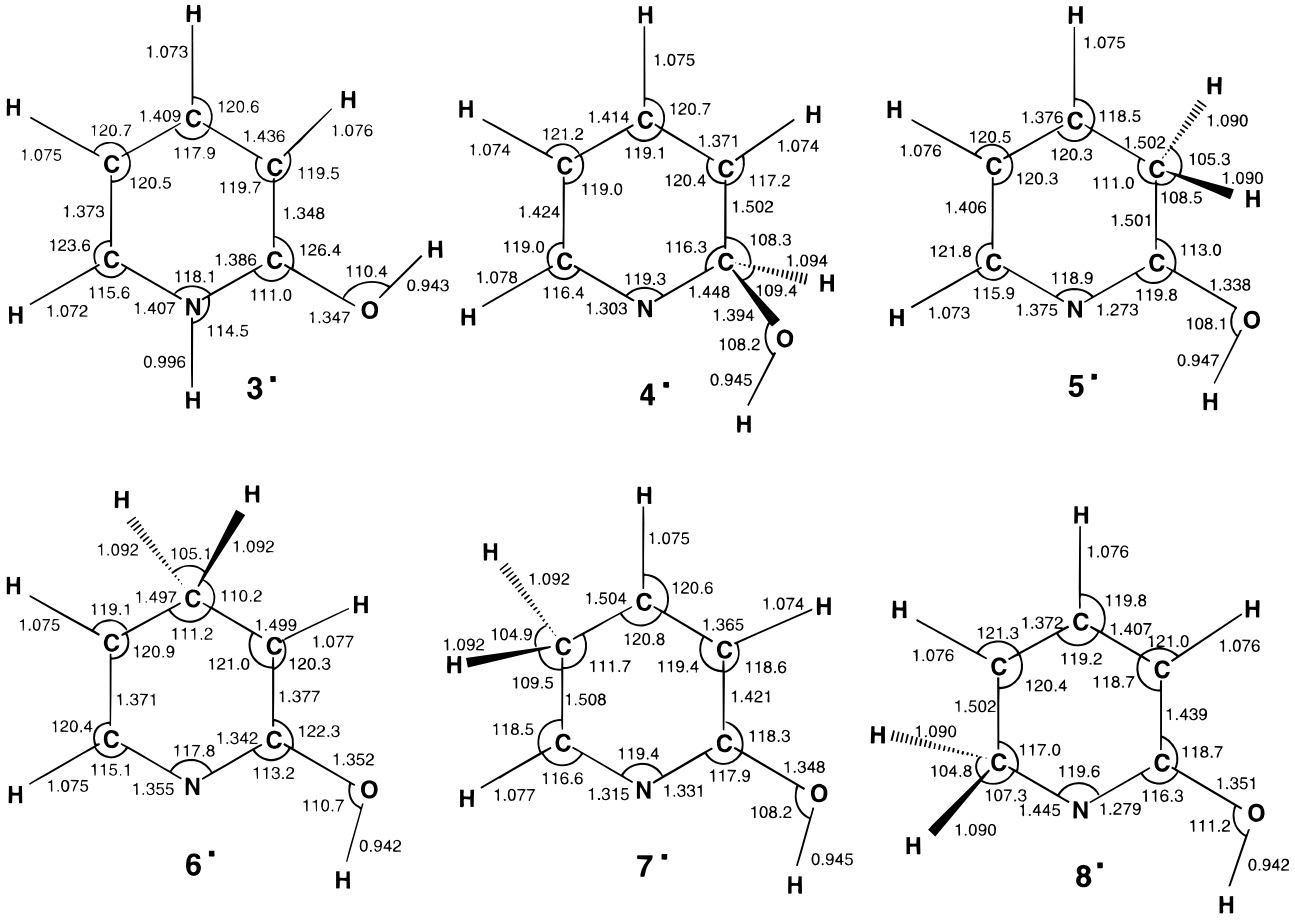

Figure 5. UHF/6-31G(d,p) optimized structures of **3**•−**8**•. Bond lengths in angstroms, bond angles in degrees.

TABLE 4: Relative Energies of Radicals 3•−15•[a]

species	PMP2[b]	B3LYP[b]	average[c]	E_{FC}[c]	ΔH_{dis}[c,d]
11•	0	0	0	32	148
14•	19	20	20	15	128
5•	35	40	37	26	103
12•	67	51	59	19	88
13•	61	59	60	51	87
7•	63	61	62	26	78
3•	68	65	67	31	74
8•	74	77	76	1	65
6•	86	86	86	19	54
4•	104	109	107	19	34
10•	145	133	139	46	8
15•[e]	149	139	144		

[a] In units of kJ mol^{-1} at 298 K. [b] Calculations with the 6-311G(2d,p) basis set, UHF/6-31G(d,p) zero-point energies, and 298 K enthalpy corrections. [c] From averaged PMP2 and B3LYP/6-311G(2d,p) energies. [d] 298 K dissociation energies to **1** or **2** and H. [e] Breaks the N−C-2 bond upon optimization.

group. The spin densities showed that the unpaired electron was mainly delocalized over the C-4 and C-6 allylic termini. Spin polarization of the β-atomic orbitals at C-5 and C-4, which resulted in negative spin densities, was related to spin contamination of the UHF wave function.[51] The slightly less stable radical **14**• was an allylic radical substituted by a weak electron withdrawing amide group, as depicted by delocalization of spin densities at C-3 and C-5 (Figure 8). The lower energy of **11**• suggested that the acylaminoallyl structure was more favorable. Likewise, radicals **13**• and **12**• contained the α-aminoalkyl and α-carbonylalkyl radical systems, as documented by localization of the spin density at C-6 and C-3, respectively. Note that in **12**•−**14**•, the electron withdrawing effect of the carbonyl oxygen resulted in substantial spin densities at the O atom (Figure 8). Radicals **12**•−**14**• thus can be viewed as containing contributions of canonical structures with oxygen-centered radicals. In general, electron-donating groups tend to stabilize alkyl radicals,[52,53] the effect of electron-withdrawing substituents is destabilizing,[54] while a combination thereof results in the stabilizing captodative effect.[55] These effects were only moderate for the acylamino group in **11**• and **13**• and the amide group in **12**• and **14**• and gave rise to only modest differences in the radical relative enthalpies (Table 4).

Radical **10**• was calculated to exist as a marginally stable structure whose dissociation to **2** and H required 8 kJ mol^{-1} at 298 K. This thermodynamic stability of **10**• was somewhat surprising because of the well-known metastability or instability of aliphatic and alicyclic hypervalent ammonium radicals.[56] However, the calculated charge and spin densities in **10**• indicated that the radical exists as a zwitterionic form[10,15] with a positively charged ammonium group (+0.20) and a dienone anion−radical system with negative charges at the oxygen atom and C-6 (Figure 9). A similar electronic structure was previously found for 2-pyrimidylammonium and 4-pyrimidylammonium radicals, which both were local energy minima, but were metastable with respect to cleavages of the N−H bonds.[10,15b] The thermodynamic stability of **10**• can be ascribed to the efficient stabilization of the negative charge by the electron-withdrawing dienone system[57] which removed the destabilizing electron density from the ammonium hydrogen atoms.[56g] The low stability of **15**• can be attributed to the facile electrocyclic opening of the dihydropyridine ring (Scheme 5).

Franck−Condon energies (E_{FC}) were also calculated for vertical electron capture in ions **3**$^+$−**14**$^+$. The E_{FC} values (Table

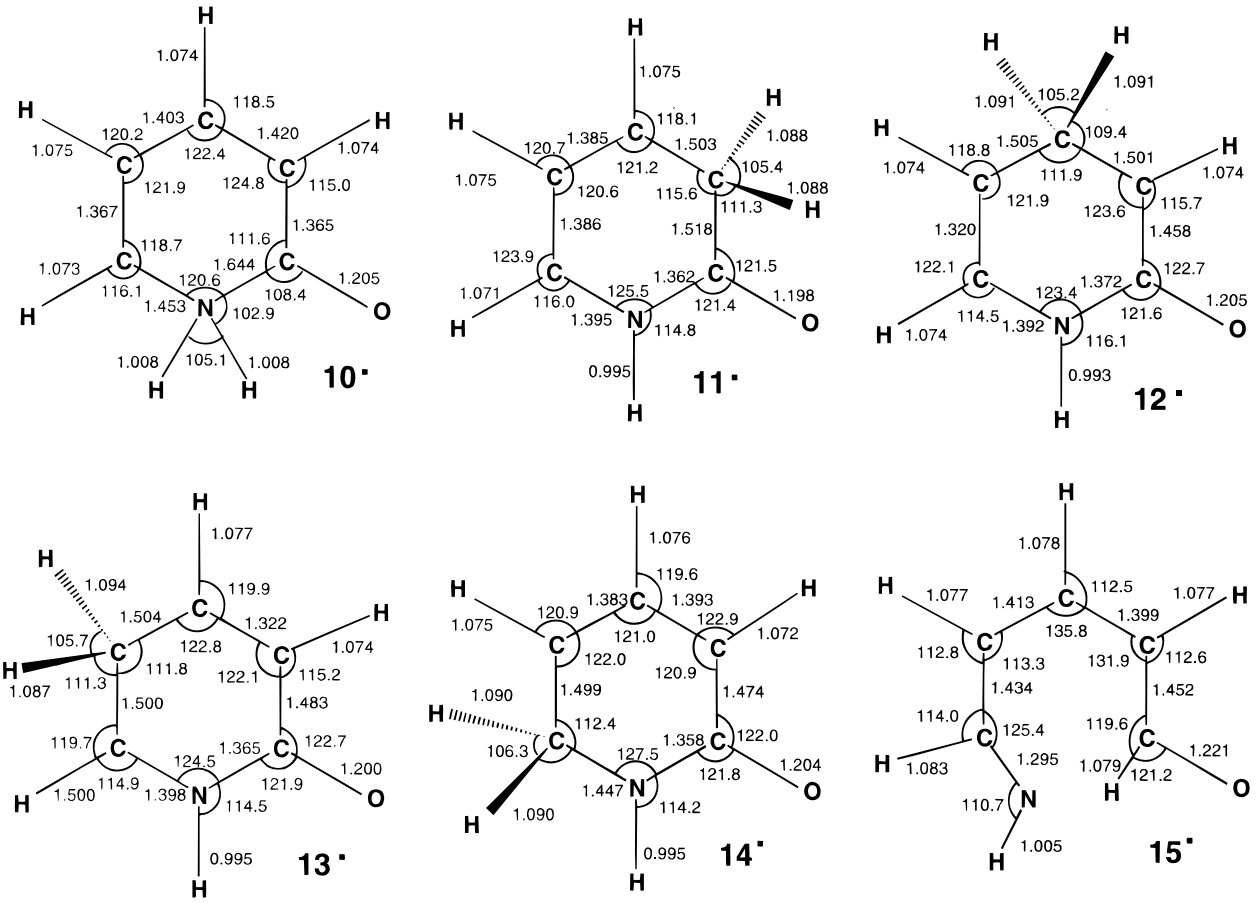

Figure 6. UHF/6-31G(d,p) optimized structures of **10**•−**15**•. Bond lengths in angstroms, bond angles in degrees.

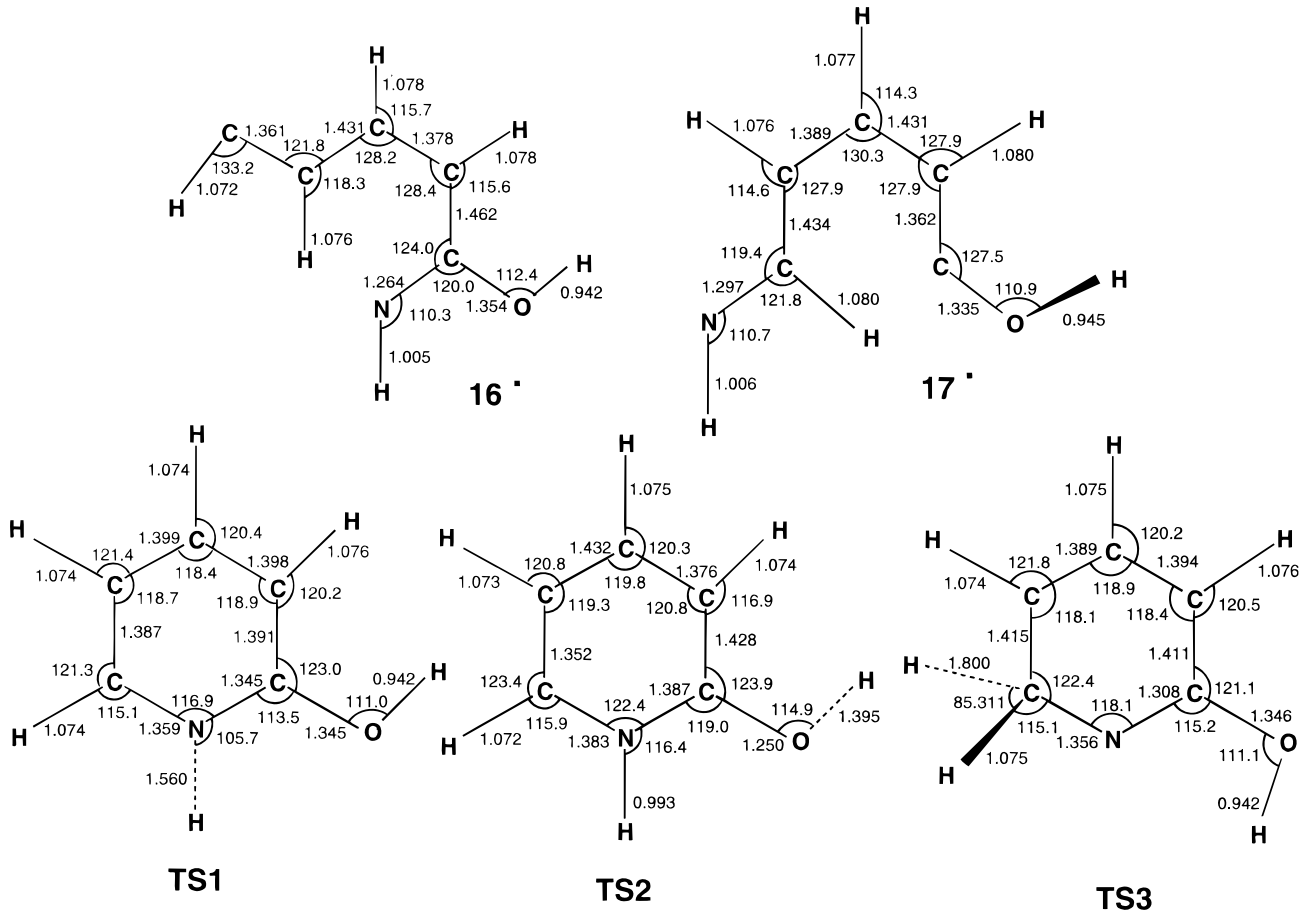

Figure 7. UHF/6-31G(d,p) optimized structures of **16**•, **17**•, **TS1**−**TS3**. Bond lengths in angstroms, bond angles in degrees.

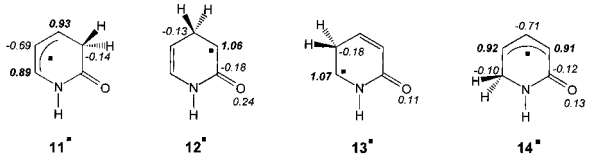

Figure 8. UHF/6-311+G(2d,p) calculated spin densities in **11**•−**14**•.

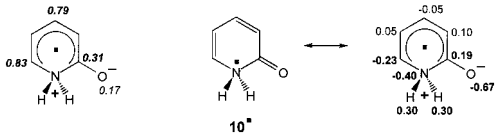

Figure 9. UHF/6-311+G(2d,p) calculated total atomic charges (roman) and spin densities (italics) in **10**•. Bold numbers show the major contributions.

SCHEME 5

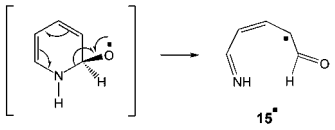

4), which gauge the mismatch between the equilibrium geometry of the ion and that of the radical, ranged between 1 kJ mol^{-1} (**8**•) and 51 kJ mol^{-1} (**13**•). In general, the Franck−Condon energies resulted from a combination of small differences in several bond lengths and angles in the pyridine ring of the cations and radicals. The Franck−Condon energy accompanying vertical ionization of **3**• was also moderate (40 kJ mol^{-1}) and by far insufficient to promote dissociation of reionized **3**$^+$.

Radicals **3**•−**8**• and **10**•−**14**• represented the isomeric products of hydrogen atom addition to **1** and **2**, respectively. The reaction enthalpies, $-\Delta H_{add} = \Delta H_{dis}$, are given in Table 4. Additions to all positions in **1** were exothermic. However, the C−H bonds in **4**•−**8**• and the N−H bond in **3**• were weak indicating that the radicals should be prone to facile dissociation to **1** unless they were kinetically stabilized by potential energy barriers to loss of H. The C−H bonds in radicals **11**•−**14**• were on average stronger than those in **3**•−**8**•, which of course reflected the greater stabilities of the former and the higher threshold for the formation of **2** compared with **1** (Table 4).

Transition State Energetics. Radical dissociations and rearrangements were also addressed by calculations to obtain the relevant potential energy barriers. The relative energies at 0 K are summarized in a potential energy profile (Figure 10). Dissociation of the N−H bond in **3**• showed a transition state at d(N−H) = 1.560 Å (**TS1**, Figure 7). The energy barrier (E_{N-H}) for **TS1** was calculated by averaged PMP2 and B3LYP and effective QCISD(T) at 120 and 136 kJ mol^{-1} above **3**•, respectively. The value of E_{N-H} depended on both the basis set and the level of correlation energy treatment (Table 5). Increasing the basis set in the PMP2 and B3LYP calculations resulted in a small increase of E_{N-H}, e.g., by 3.7 kJ mol^{-1} for PMP2 energies calculated with the 6-31G(d,p) and 6-311+G-(2d,p) basis sets. The QCISD(T) energy showed another increase by 12.5 kJ mol^{-1} compared with the PMP2 energy. Interestingly, the B3LYP and PMP2 values for E_{N-H} were practically identical for the larger basis sets used (Table 5). The calculations also pointed to a substantial activation energy for the addition of a

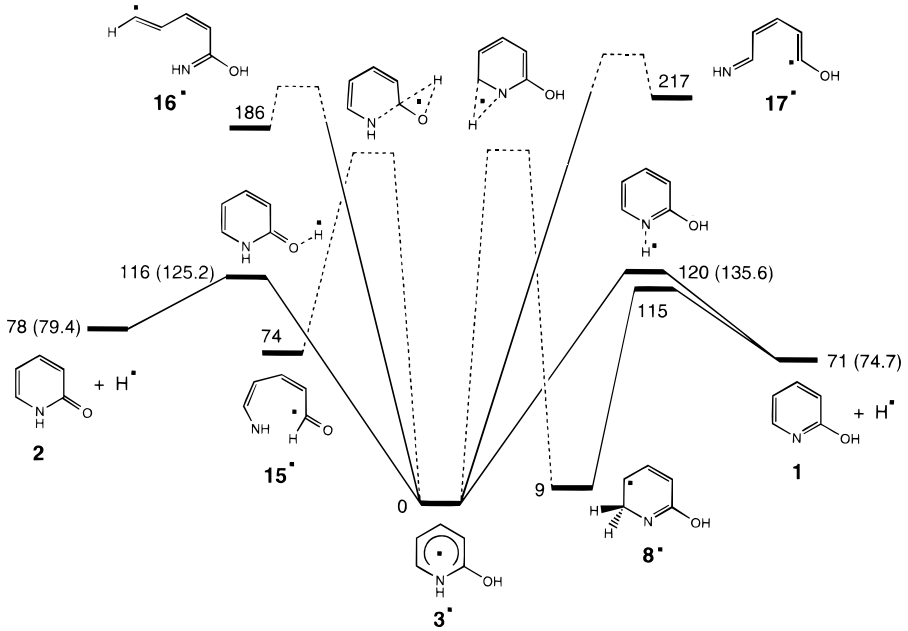

Figure 10. Potential energy profile for dissociations and isomerizations of **3**•. The energies are from combined PMP2/B3LYP/6-311G(2d,p) calculations. Values in parentheses are from effective QCISD(T)/6-311+G(2d,p) calculations.

TABLE 5: Transition State and Dissociation Energies

	energy[a]				
species	PMP2 6-31G(d,p)	PMP2 B3LYP 6-311G(2d,p)	PMP2 B3LYP 6-311+G(2d,p)	QCISD(T) 6-31G(d,p)	QCISD(T)[b] 6-311+G(2d,p)
TS1	119	119 120	123 124	132	136
TS2	126	124 107	121 107	130	125
1 + H[c]	50	53 94	58 98	70	78
2 + H[c]	63	66 96	70 99	77	83

[a] In kJ mol^{-1} relative to **3**• including zero-point corrections. [b] Effective values from eq 1. [c] At 298 K including thermal vibrational, rotational, and translational corrections.

hydrogen atom to the nitrogen atom in **1**, $E_{N+H} = 48$ and 61 kJ mol^{-1} by averaged PMP2/B3LYP and QCISD(T) calculations, respectively. The dissociation energy of the N−H bond in **3**$^{\bullet}$ at 298 K, BDE(N−H), was calculated as 74 and 78 kJ mol^{-1} by the two methods used (Table 5).

Dissociation of the O−H bond in **3**$^{\bullet}$ reached an early transition state at d(O−H) = 1.395 Å (**TS2**, Figure 7). The **TS2** energy (E_{O-H}) was calculated at 116 and 125 kJ mol^{-1} above **3**$^{\bullet}$ by the averaged PMP2/B3LYP and QCISD(T), respectively (Figure 10). The different values of E_{O-H} at different levels of ab initio theory resulted from a combination of several factors. First, the B3LYP activation energies were systematically 14−16 kJ mol^{-1} lower than those from the PMP2 calculations (Table 5). Increasing the basis set resulted in a slight (0.5 kJ mol^{-1}) lowering of the E_{O-H}, while improving the correlation energy treatment by QCISD(T) increased the E_{O-H} by 4 kJ mol^{-1} (Table 5). The calculated E_{O-H} provided the activation energy for the addition of a hydrogen atom to the carbonyl oxygen in **2**, $E_{O+H} = 38$ and 46 kJ mol^{-1}, respectively for the two sets of calculations. It is noteworthy that the transition states for both the O−H bond cleavage and formation had lower energies than the corresponding ones for the N−H bond cleavage and formation. These small energy differences affected the kinetics of the competing dissociations of **3**$^{\bullet}$ and additions of H to **1** and **2**, as discussed below.

A transition state was also sought for hydrogen migrations that would isomerize **3**$^{\bullet}$ to **8**$^{\bullet}$ and **11**$^{\bullet}$. The potential energy surface for the migration of the N−H hydrogen to C-6 was mapped systematically by UHF/6-31G(d,p) calculations for fixed N···H distances between 1.45 and 2.1 Å. The relevant part of the potential energy surface consisted of a valley along the N−H dissociation coordinate reaching a saddle point at d(N−H) = 1.560 Å (**TS1**, vide supra) and another valley along the C-6−H dissociation coordinate. The latter had a saddle point at d(C-6−H) = 1.80 Å (**TS3**, Figure 7), corresponding to a late transition state for C-6−H bond cleavage which was 106 kJ mol^{-1} above **8**$^{\bullet}$ (Figure 10). The valleys were separated by a ridge whose height decreased continuously with increasing the N···H and C-6...H distances. Even at d(N−H) = 2.1 Å the crest of the ridge showed a negative gradient along the N···H coordinate. This indicated that attempts by **3**$^{\bullet}$ to climb the ridge en route to rearrangement to **8**$^{\bullet}$ would instead accelerate the motion along the N···H dissociation coordinate and lead to dissociation. Single-point calculations of the crest energy at d(N−H) = 1.560 Å yielded $\Delta E = 74$ kJ mol^{-1} which was the height of the ridge above **TS1**. A frequency analysis at this point showed two imaginary frequencies. The calculations indicated that, barring efficient tunneling, a 1,2-hydrogen rearrangement from N to C-6 was energetically impossible in **3**$^{\bullet}$ up to 74 kJ mol^{-1} above the transition state for dissociation. In addition, even if a first-order saddle point had existed at some larger N···H distance, the rearrangement would have been dynamically disfavored, because the repulsive part of the potential energy surface past **TS1** imparted translational energy to the departing hydrogen atom to move along the N···H coordinate.

A transition state for the 1,3-migration of the O−H hydrogen atom to C-3 in **3**$^{\bullet}$ was also investigated by UHF/6-31G(d,p) calculations. Upon moving the hydrogen atom toward C-3, the potential energy surface showed a negative energy gradient along the O−H coordinate for all O..H distances investigated 1.35−2.1 Å. The gradient decreased with the increasing O···H distance, but at all points it indicated O···H bond dissociation. No first-order saddle point was found for the hydrogen migration; in contrast, the potential energy surface along the attempted rearrangement pathways was repulsive in the O···H coordinate and if accessed it would result in dissociation rather than rearrangement. It can be concluded that a **3**$^{\bullet}$ → **11**$^{\bullet}$ rearrangement was kinetically disfavored against dissociation to **2** and a hydrogen atom.

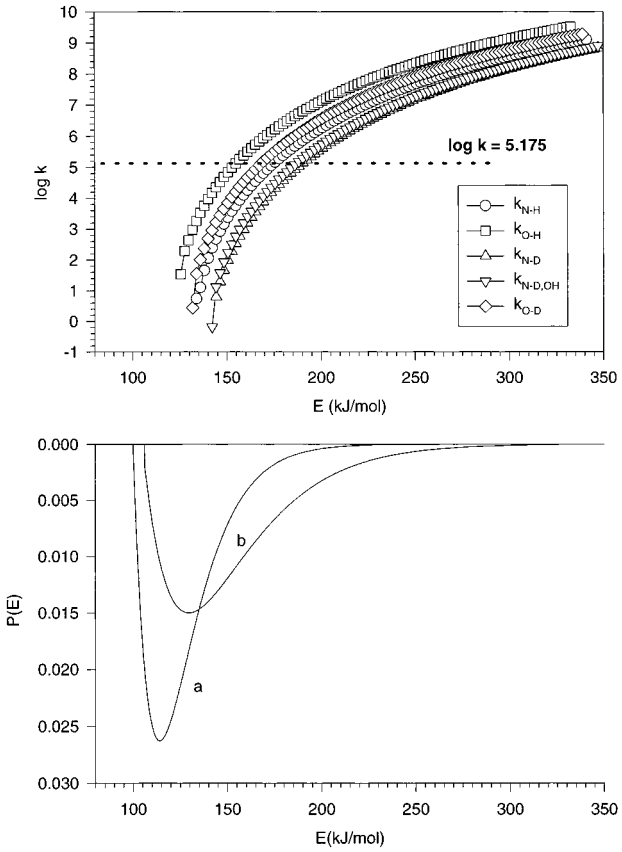

Figure 11. RRKM calculated unimolecular rate constants for the loss of H and D from **3**$^{\bullet}$ and **3D$_2$**$^{\bullet}$ and the best-fit energy distribution function. The rate constants are based on the effective QCISD(T)/6-311+G(2d,p) activation energies, UHF/6-31G(d,p) moments of inertia, and scaled harmonic frequencies.

Dissociation Kinetics. The calculated activation energies allowed us to estimate the unimolecular rate constants (k_{uni}) for N−(H,D) and O−(H,D) bond dissociations in **3**$^{\bullet}$ and its isotopomers and to assess the pertinent isotope effects. Since the activation energies obtained at the various levels of theory differed by several kJ mol^{-1}, the RRKM calculated rate constants differed by 2−3 orders of magnitude for the different sets of energies. However, relative rate constants for the competitive losses of the N−H and O−H hydrogen atoms showed consistent trends as did the calculated isotope effects.

The calculated log k_{uni} for the N−H and O−H bond dissociations in **3**$^{\bullet}$ are shown in Figure 11. Both sets of calculations predicted moderate kinetic shifts (ΔE_{kin}) for the dissociations. The kinetic shifts were due to the fact that achieving dissociation on the time scale of the measurements (4.67 μs) required appropriate k_{uni}, e.g., log $k_{uni} = 5.17$ for 50% dissociation. On the basis of the combined PMP2/B3LYP and QCISD(T) calculations, 50% dissociation of **3**$^{\bullet}$ by cleavage of the O−H bond was expected to show $\Delta E_{kin} = 24$ and 30 kJ mol^{-1}, respectively. This extra energy provided additional kinetic stabilization for **3**$^{\bullet}$ with internal energies between $E_{a,O-H}$ (116−125 kJ mol^{-1}) and $E_{a,O-H} + \Delta E_{kin}$ (140−156 kJ mol^{-1}).

To evaluate the RRKM rate constants, kinetic isotope effects were calculated for the various combinations of H and D losses from **3-D$_2$**$^{\bullet}$, **3-OD**$^{\bullet}$, and **3-ND**$^{\bullet}$ and compared with experiment.

The calculated k_{uni} for the N−H and O−H bond cleavages in **3•**, denoted as k_{N-H} and k_{O-H}, respectively, and N−D and O−D bond cleavages in **3-D$_2$•**, denoted as k_{N-D} and k_{O-D}, respectively, were population averaged with a Boltzmann-like internal-energy distribution function, *P(E)* (eq 4)[15a] and used to calculate the flux of radicals nondissociating on the time scale of the experiment (τ = 4.67 μs, eqs 5−6). A single distribution function was considered for **3•** and **3-D$_2$•** to simplify the calculations.

$$P(E) = \frac{4(E - E_0)}{W^2} e^{-2(E-E_0)/W} \quad (4)$$

$$[\mathbf{3}] = \{[\mathbf{3}] + [\mathbf{3} - \mathbf{H}]\} \int_0^{\infty} P(E) e^{-(k_{N-H}+k_{O-H})\tau} dE \quad (5)$$

$$[\mathbf{3D}_2] = \{[\mathbf{3D}_2] + [\mathbf{3D}_2 - \mathbf{D}]\} \int_0^{\infty} P(E) e^{-(k_{N-D}+k_{O-D})\tau} dE \quad (6)$$

Since loss of H from the hydroxyl group in **3•** to yield **2** was the lowest energy dissociation (Figure 10), the kinetics was evaluated from the fluxes of **3•** and **2** and similarly for the labeled derivatives. The fluxes were presumed to be proportional to the integrated peak intensities in the NR spectra, e.g., [**3•**] at *m*/*z* 96, [**3-D$_2$•**] at *m*/*z* 98, [**1,2**] at *m*/*z* 95, and [**2-ND**] at *m*/*z* 96. This presumed that **3•** and **2** had similar ionization cross sections. Such an assumption was reasonably justified by the fact that ionization cross sections in general scale with the number of atoms, and **3•** and **2** differed by a single hydrogen atom which contributed a small increment.[58] Another assumption inherent to this treatment of dissociation kinetics was that the consecutive dissociations of reionized **3**$^+$ and **2**$^{+\bullet}$ occurred to a similar extent, so the measured relative abundances were not skewed by subsequent ion dissociations. The calculated [**3**] and [**3-D$_2$**] relative intensities were least-squares fitted to the experimental relative abundances of the corresponding NR ions. The latter were taken from the NR spectra of precursors generated by low-energy protonation with NH_4^+ or deuteronation-exchange with ND_3/ND_4^+, e.g., [**3**]/{[**3**] + [**2**]} = 0.498 and [**3-D$_2$**]/{[**3-D$_2$**] + [**2-ND**]} = 0.623. The fits yielded the width (*W*) and position (E_0) parameters for the internal energy distribution function. The best fit for k_{uni} based on the QCISD(T) calculated energies was W = 49 kJ mol^{-1} and E_0 = 105 kJ mol^{-1}, which gave [**3**]/{[**3**] + [**2**]} = 0.496 and [**3-D$_2$**]/{[**3-D$_2$**] + [**2-ND**]} = 0.621. The best fit for k_{uni} based on the PMP2/B3LYP calculated energies was W = 28 kJ mol^{-1} and E_0 = 100 kJ mol^{-1}. The *P(E)* functions (Figure 11) showed maxima, $E_{max} = E_0 + W/2$, at E_{max} = 129 and 114 kJ mol^{-1} and full widths at half-maximum, ΔE_{fwhm} = 59 and 34 kJ mol^{-1}, respectively. The calculated energy distribution maxima were reasonable as followed from an energy analysis. The internal energy in **3•** (E_{int}) was composed of the internal energy in the precursor ion (**3**$^+$) and the Franck−Condon energy upon neutralization (E_{FC} = 31 kJ mol^{-1}, Table 4). The ion energy consisted of the thermal energy in the precursor molecules (38 kJ mol^{-1} at 200 °C) and a 85% fraction of the protonation exothermicity according to the calculations of Uggerud.[59] The latter was estimated by Boltzmann-averaging PA(**1**) − PA(NH_3) = 69 kJ mol^{-1} and PA(**2**) − PA(NH_3) = 76 kJ mol^{-1} over the populations of **1** (73%) and **2** (27%) at the ion source temperature (200 °C). The estimate yielded an average E_{int} = 129 kJ mol^{-1} in **3•** in close agreement with the *P*(*E*) maximum obtained by fitting the QCISD(T) energies (129 kJ mol^{-1}, vide supra). A similar estimate was made for the energy distribution in **3•** prepared by neutralization of **3**$^+$ from the more exothermic protonation with $(CH_3)_2C{-}OH^+$, $E_{int} \leq$ 164 kJ mol^{-1}.

It should be noted that the estimated E_{int} represented an upper energy bound, because the precursor ions underwent several tens of collisions with the NH_3 reagent gas in the ion source. However, recent measurements of intermolecular energy transfer by Dai et al.[60] indicated that the energy transferred per collision becomes very small (<50 cm^{-1}) for hot molecules with internal energies below ca. 200 kJ mol^{-1}. It is therefore probable that moderate vibrational excitation in **3**$^+$ attained by exothermic protonation was not depleted substantially by ion−molecule collisions.

The internal energy distribution functions, when convoluted with the RRKM rate constants, further allowed us to calculate branching ratios for the formation of **1** and **2** by competitive dissociations of **3•**. The neutral fluxes of **1** and **2** were expressed by eq 7 and 8, respectively. The formations of **1-OD** and **2-ND** from **3-D$_2$•** followed similar equations, where τ = 4.72 μs, and the pertinent k_{uni} were k_{N-D} and k_{O-D}. The k_{N-H}/k_{O-H} branching ratios calculated with using the QCISD(T) energies did not depend strongly on the internal energy distribution in **3•**, e.g., k_{N-H}/k_{O-H} = 0.101 and 0.108 for E_{max} = 129 and 164 kJ mol^{-1}, respectively. The branching ratios were also very similar for dissociations of the labeled radicals **3-D$_2$•**, e.g., k_{N-D}/k_{O-D} = 0.097 and 0.102 for E_{max} = 129 and 164 kJ mol^{-1}, respectively. The branching ratios based on the combined PMP2/B3LYP energies gave somewhat higher values, e.g., k_{N-H}/k_{O-H} = 0.289 and 0.306 for E_{max} = 114 and 149 kJ mol^{-1},

$$[\mathbf{1}] = \int_0^{\tau} k_{N-H}[\mathbf{3}]dt = \int_0^{\tau} dt \int_0^{\infty} P(E) k_{N-H}(E) e^{-(k_{N-H}+k_{O-H})\tau} dE \quad (7)$$

$$= \int_0^{\infty} \frac{k_{N-H}(E)}{k_{N-H}(E) + k_{O-H}(E)} P(E)[1 - e^{-(k_{N-H}+k_{O-H})\tau}]dE$$

$$[\mathbf{2}] = \int_0^{\tau} k_{O-H}[\mathbf{3}]dt = \int_0^{\tau} dt \int_0^{\infty} P(E) k_{O-H}(E) e^{-(k_{N-H}+k_{O-H})\tau} dE \quad (8)$$

$$= \int_0^{\infty} \frac{k_{O-H}(E)}{k_{N-H}(E) + k_{O-H}(E)} P(E)[1 - e^{-(k_{N-H}+k_{O-H})\tau}]dE$$

respectively. Hence, both sets of calculations predicted preferential formation of **2** upon the lowest energy dissociation of **3•**. The higher level QCISD(T) energies predicted a higher specificity in the formation of **2** from **3•**.

Excited States of 3•. The potential-energy surface for the ground electronic state in **3•** clearly indicated that loss of H to form **2** and **1** should be the lowest energy dissociations (Figure 10). However, the NR mass spectrum of **3•** showed substantial formations of small fragments due to ring-cleavage dissociations. The latter could not be entirely accounted for by *consecutive* dissociations of **1**,**2** or **1,2**$^{+\bullet}$, because the latter showed much less dissociation upon NR (Figure 2a). It was also clear that the internal energy distribution in **3•** dissociating by loss of H did not allow formation of hot **2** and **1** to promote consecutive ring-cleavage dissociations in neutral molecules or cation radicals formed by collisional ionization. Dissociations of reionized **3**$^+$ proceeded mostly by elimination of water, whereas products of ring-cleavage dissociations were less abundant (Figure 1). This pointed to the possibility of ring-cleavage dissociations in **3•**. However, to be competitive with the H loss, the ring cleavages must occur in very hot radicals of E_{int} >

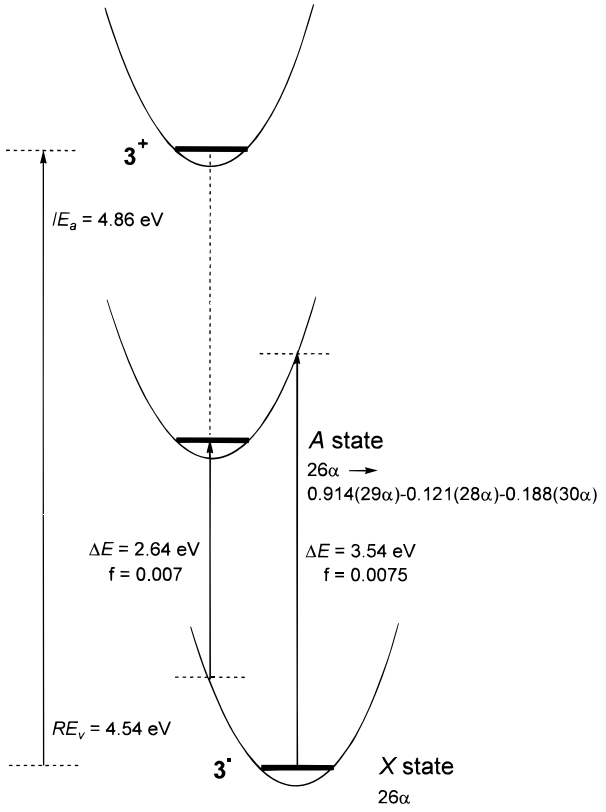

Figure 12. Potential energy diagram for the *X* and *A* states in **3•**. Excitation energies and oscillator strengths are from CIS/6-311G(2d,p) calculations, adiabatic ionization (IE_a) and vertical recombination (RE_v) energies are from combined PMP2/B3LYP/6-311G(2d,p) calculations.

220 kJ mol^{-1} (Figure 10), which appeared to be incompatible with the internal energy distributions derived from the isotope effects on loss of H and D. A possible mechanism for energy deposition in a fraction of **3•** was through excited electronic states formed upon collisional electron transfer. Since the latter process is nonresonant the electron can be captured in any of the manifold of unoccupied orbitals to form the ground or an excited electronic state of the radical. Only those excited states can be kinetically significant that have enough energy for ring-cleavage dissociations to occur and that also have radiative lifetimes compatible with the time scale of the dissociations.

The five lowest excited states in **3•** were investigated with CIS/6-311G(2d,p) calculations for radicals formed by vertical electron transfer and for those with the relaxed geometry of the ground (X) state. The use of CIS was justified by the substantial energy gap between the doubly occupied 25α orbital and the singly occupied 26α SOMO ($\Delta E = 3.89$ eV), which was greater than the X→A excitation energy (3.54 eV). Single-electron excitations in **3•** therefore could involve electron promotion from the 26α SOMO to the appropriate combination of virtual orbitals. Such "outer" excited states were also expected to be formed upon vertical electron capture in $\mathbf{3}^+$. The properties of the first excited state in **3•** are shown in Figure 12. The potential energy surfaces for the X and A states were shifted, such that the excitation energy in relaxed (*X*)**3•**, $\Delta E = 3.54$ eV was greater than in **3•** formed by vertical neutralization of ion $\mathbf{3}^+$, $\Delta E =$ 2.64 eV. This shift may facilitate internal conversion of the A state to vibrationally excited *X* state, because of the proximity of the potential energy surfaces.[61] The available energy (255 kJ mol^{-1}) was sufficient to promote ring opening in **3•** (Figure 10). In addition, the calculated radiative lifetime of the A state, $\tau_{ij} = 1/A_{ij} = 0.47$ μs, was sufficiently long to allow ring-cleavage dissociations proceeding directly from the A state. Two higher states, B and C, of $\Delta E = 3.98$ and 4.43 eV, respectively, were also outer excited states due to promotion of the 26α electron to combinations of the 27α through 30α virtual orbitals. The calculated radiative lifetimes were 4.8 and 2.3 μs for the B and C states, respectively, which were sufficient for unimolecular dissociations to occur. Figure 12 also shows the calculated adiabatic ionization energy of **3•** at 0 K, $IE_a = 4.86$ eV from combined PMP2/B3LYP/6-311G(2d,p) calculations.

Although the details of the potential energy surfaces for the A, B, C, and higher excited electronic states were unknown, the excitation energies and radiative lifetimes suggested that highly endothermic ring dissociations could occur in vertically neutralized **3•**. Internal conversion of the excited states to the X state can be expected to produce the latter with a bimodal distribution of internal energy. The low-energy part of the *P*(*E*) function is due to the Franck−Condon effects in the formation of the X state and the precursor ion internal energy, as discussed above. The high-energy part of the *P*(*E*) function is governed by the energy gap between the excited state and ground state of **3•**.

Conclusions

The experimental and computational data were in accord that the 2-hydroxy-(1H)pyridinium radical (**3•**) was a stable species in the gas phase. Hydrogen atom additions to the N-atom in 2-hydroxypyridine (**1**) and to the carbonyl oxygen atom in 2-(1H)pyridone (**2**) were associated with potential energy barriers. Addition of a hydrogen atom to **2** was found to be energetically preferred. Radicals **3•** acquired a bimodal internal energy distribution when formed by collisional electron transfer in the gas phase. The low-energy part of the energy distribution function was composed of the internal energy of the precursor ion and the Franck−Condon energy upon vertical electron transfer. The high-energy part of the energy distribution was due to the formation of long-lived outer excited states that either dissociated adiabatically by ring-cleavage or underwent internal conversion to a vibrationally excited ground electronic state. This study and that of the related 3-hydroxy-(1H)pyridinium radical[15b] pointed out that bimodal energy distributions in molecules and radicals due to populations of excited electronic states upon femtosecond collisional electron transfer may be more common than previously recognized.

Acknowledgment. Support of this work by the National Science Foundation (Grant CHE-9712570) is gratefully acknowledged. Computational support was provided by the University of Washington Computing and Communications Center and the Department of Chemistry Computer Cluster. We thank Dr. David Hrovat for the orbital visualization program.

Supporting Information Available: Tables of HF/6-31G-(d,p) optimized geometries (Cartesian coordinates), uncorrected harmonic frequencies, and total energies. Supporting Information is available free of charge via the Internet at http://pubs.acs.org.

References and Notes

(1) (a) Kuzuya, M.; Noguchi, A. *Trends Org. Chem.* **1991**, *2*, 73−92. (b) Katritzky, A. R.; Karelson, M.; Harris, P. A. *Heterocycles*, **1991**, *32*, 329. (c) Les, A.; Kukawska-Tarnawska, B. *THEOCHEM* **1986**, *33*, 45−60.

(2) (a) Inuzuka, K. *Nippon Kagaku Kaishi* **1998**, 149−156. (b) Kwiatkowski, J. S.; Leszczynski, J. *J. Mol. Struct.* **1996**, *376*, 325−342. (c) Spoliti, M.; Bencivenni, L.; Diomedi-Carmassei, F.; D'Alessio, L. *Rass. Chim* **1993**, *45*, 143−150; *Chem. Abstr.* **1995**, *123*, 339007. (d) Kwiatkowski, J. S.; Leszczynski, J. *THEOCHEM* **1994**, *118*, 201−213. (e) Les, A.; Adamowicz, L.; Nowak, M., J.; Lapinski, L. *THEOCHEM* **1994**, *118*,

157−166. (f) Rendell, A. P.; Guest, M. F.; Kendall, R. A. *J. Comput. Chem.* **1993**, *14*, 1429−1439. (g) Parchment, O. G.; Burton, N. A.; Hillier, I. H.; Vincent, M. A. *J. Chem. Soc., Perkin Trans. 2* **1993**, 861−863. (h) Les, A.; Adamowicz, L.; Nowak, M., J.; Lapinski, L. *THEOCHEM* **1992**, *96*, 313−327. (i) Parchment, O. G.; Burton, N. A.; Hillier, I. H. *Chem. Phys. Lett.* **1993**, *203*, 46−48. (j) Facelli, J. C.; Orendt, A. M.; Contreras, R. H.; Tufro, M. F.; DeKowalewski, D. G. *J. Phys. Chem.* **1992**, *96*, 7895−7898. (k) Moreno, M.; Miller, W. H. *Chem. Phys. Lett.* **1990**, *171*, 475−479. (l) Adamowicz, L. *Chem. Phys. Lett.* **1989**, *161*, 73−78. (m) Kwiatkowski, J. S.; Bartlett, R. J.; Person, W. B. *J. Am. Chem. Soc.* **1988**, *110*, 2353−58. (n) Les, A.; Ortega-Blake, I. *Int. J. Quantum Chem.* **1986**, *30*, 225−237. (o) Scanlan, M. J.; Hillier, I. H. *Chem. Phys. Lett.* **1984**, *107*, 330−332.

(3) (a) Pomellia, C. S.; Tomasi, J. *THEOCHEM.* **1998**, *433*, 151−160. (b) Hung, F.-T. *Huaxue* 1997, *55*, 95−104. *Chem. Abstr.* **1998**, *129*, 15870. (c) Barone, V.; Cossi, M.; Tomasi, J. *J. Comput. Chem.* **1998**, *19*, 404−417. (d) Chou, P.-T.; Wei, C.-Y.; Hung, F.-T. *J. Phys. Chem. B* **1997**, *101*, 9119−9126. (e) Wang, J.; Boyd, R. J. *J. Phys. Chem.* **1996**, *100*, 16141. (f) Wang, J.; Boyd, R. J. *Chem. Phys. Lett.* **1996**, *259*, 647−653. (g) Luque, F. J.; Bachs, M.; Aleman, C.; Orozco, M. *J. Comput. Chem.* **1996**, *17*, 806−820. (h) Luque, F. J.; Zhang, Y.; Aleman, C.; Bachs, M.; Gao, J.; Orozco, M. *J. Phys. Chem.* **1996**, *100*, 4269−4276. (i) Adamo, C.; Lelj, F. *Int. J. Quantum. Chem.* **1995**, *56*, 645−653. (j) Gao, J.; Shao, L. *J. Phys. Chem.* **1994**, *98*, 13772−13779. (k) Michel, A. G.; Trudel, Y.; Dion, C. *Int. J. Quantum. Chem.* **1993**, *46*, 183−190. (l) Wong, M. W.; Wiberg, K. B.; Frisch, M. J. *J. Am. Chem. Soc.* **1992**, *114*, 1645−52. (m) Cieplak, P.; Singh, U. C.; Kollman, P. A. *Int. J. Quantum. Chem., Quantum Biol. Symp.* **1987**, *14*, 65−74. (n) Cieplak, P.; Singh, U. C.; Kollman, P. A. *J. Am. Chem. Soc.* **1987**, *109*, 6283−89. (o) Field, M. J.; Hillier, I. H. *J. Chem. Soc., Perkin Trans. 2* **1987**, 617−622. (p) Lledos, A.; Bertran, J. *THEOCHEM* **1985**, *21*, 73−78. (q) Field, M. J.; Hillier, I. H.; Guest, M. F. *J. Chem. Soc., Chem. Commun.* **1984**, 1310−11.

(4) (a) Sobolewski, A. L.; Adamowicz, L. *Chem. Phys.* **1996**, *213*, 193−201. (b) Sobolewski, A. L.; Adamowicz, L. *J. Chem. Phys.* **1996**, *100*, 3933−3941. (c) Barone, V.; Adamo, C. *Chem. Phys. Lett.* **1994**, *226*, 399−404. (d) Barone, V.; Adamo, C. *J. Photochem. Photobiol., A* **1994**, *80*, 211−219. (e) Barone, V.; Adamo, C. *J. Comput. Chem.* **1994**, *15*, 395−404. (f) Sobolewski, A. L. *Chem. Phys. Lett.* **1993**, *211*, 293−299. (g) Adamo, C.; Barone, V.; Loison, S.; Minichino, C. *J. Chem. Soc., Perkin Trans. 2* **1993**, 697−702. (h) Kwiatkowski, J. S.; Tempczyk, A. *Chem. Phys.* **1984**, *85*, 397−402.

(5) See for example: (a) Mirkin, S. M. *Annu. Rev. Biophys. Biomol. Struct.* **1995**, *24*, 319. (b) Sinden, R. R. *DNA Structure and Function*; Academic Press: San Diego, 1994. (c) Costas, M. E.; Acevedo-Chavez, R. *J. Phys. Chem. A* **1997**, *101*, 8309 and references therein.

(6) For reviews, see: (a) Glass, W. A.; Varma, M. N., Eds. *Physical and Chemical Mechanisms in Molecular Radiation Biology*; Plenum Press: New York, 1991. (b) Richter, C. In *Free Radical Toxicology*; Wallace, K. B., Ed.; Taylor and Francis: Washington, DC, 1997.

(7) (a) von Sonntag, C. In *Physical and Chemical Mechanisms in Molecular Radiation Biology*; Glass, W. A., Varma, M. N., Eds.; Plenum Press: New York, 1991; pp 287−321. (b) Steenken, S. *Chem. Rev.* **1989**, *89*, 503.

(8) Nguyen, V. Q.; Turecek, F. *J. Mass Spectrom.* **1996**, *31*, 1173.

(9) Nguyen, V. Q.; Turecek, F. *J. Mass Spectrom.* **1997**, *32*, 55.

(10) Nguyen, V. Q.; Turecek, F. *J. Am. Chem. Soc.* **1997**, *119*, 2280.

(11) Turecek, F. *J. Mass Spectrom.* **1998**, *33*, 779.

(12) For reviews, see: (a) Wesdemiotis, C.; McLafferty, F. W. *Chem. Rev.* **1987**, *87*, 485. (b) Terlouw, J. K.; Schwarz, H. *Angew. Chem., Int. Ed. Engl.* **1987**, *26*, 805. (c) Holmes, J. L. *Mass Spectrom. Rev.* **1989**, *8*, 513. (d) Terlouw, J. K. *Adv. Mass Spectrom.* **1989**, *11*, 984. (e) McLafferty, F. W. *Science* **1990**, *247*, 925. (f) Turecek, F. *Org. Mass Spectrom.* **1992**, *27*, 1087. (g) Goldberg, N.; Schwarz, H. *Acc. Chem. Res.* **1994**, *27*, 347. (h) Schalley, C. A.; Hornung, G.; Schroder, D.; Schwarz, H. *Chem. Soc. Rev.* **1998**, *27*, 91.

(13) Sadilek, M.; Turecek, F. *J. Phys. Chem.* **1996**, *100*, 224.

(14) (a) Kuhns, D. W.; Shaffer, S. A.; Tran, T. B.; Turecek, F. *J. Phys. Chem.* **1994**, *98*, 4845. (b) Kuhns, D. W.; Turecek, F. *Org. Mass Spectrom.* **1994**, *29*, 463.

(15) (a) Turecek, F.; Wolken, J. K. *J. Phys. Chem. A* **1999**, *103*, 1905. (b) Wolken, J. K.; Turecek, F. *J. Am. Chem. Soc.* **1999**, *121*. In press.

(16) (a) Beak, P. *Acc. Chem. Res.* **1977**, *10*, 186. (b) Smets, J.; Maes, G. *Chem. Phys. Lett.* **1991**, *187*, 532−536. (c) Nowak, M. J.; Lapinski, L.; Fulara, J.; Les, A.; Adamowicz, L. *J. Phys. Chem.* **1992**, *96*, 1562−69. (d) Lapinski, L.; Nowak, M. J.; Fulara, J.; Les, A.; Adamowicz, L. *J. Phys. Chem.* **1992**, *96*, 6250−54.

(17) (a) Kaminski, G. A.; Jorgensen, W. L. *J. Phys. Chem. B*, **1998**, *102*, 1787−1796. (b) Bakulev, V. A.; Biryucheva., N. Yu.; Pichko, V. A. *Chem. Heterocycl. Compd.* **1997**, *33*, 99−105. (c) Shishkin, O. V. *Izv. Akad. Nauk, Ser. Khim.* **1996**, 2650−2652. (d) Maran, U.; Karelson, M.; Katritzky, A. R. *Int. J. Quantum. Chem.* **1996**, *60*, 41−49. (e) Orozco, M.; Bachs, M.; Luque, F. J. *J. Comput. Chem.* **1995**, *16*, 563−570. (f) Ashok, R. N. K. *Proc. Indian Acad. Sci., Chem. Sci.* **1994**, *106*, 163−168. *Chem. Abstr.* **1995**, *121*, 156908. (g) Szafran, M.; Karelson, M.; Katritzky, A. R.; Koput, J.; Zerner, M. C. *J. Comput. Chem.* **1993**, *14*, 371−377. (h) Fabian, W. M. F. *J. Comput. Chem.* **1991**, *12*, 17. (i) Rzepa, H. S.; Yi, M. Y.; Karelson, M. M.; Zerner, M. C. *J. Chem. Soc., Perkin Trans. 2* **1991**, 635−637. (j) Fabian, W. M. F. *J. Phys. Org. Chem.* **1990**, *3*, 332−338. (k) Millefiori, S.; Millefiori, A. *Bull. Chem. Soc. Jpn.* **1990**, *63*, 2981−84. (l) Karelson, M. M.; Katritzky, A. R.; Szafran, M.; Zerner, M. C. *J. Org. Chem.* **1989**, *54*, 6030. (m) Sygula, A. *Journal of Chemical Research Synopses* **1989**, 56−57. (n) Katritzky, A. R.; Szafran, M.; Stevens, J. *THEOCHEM* **1989**, *53*, 179−192. (o) Saunders: M.; Webb, G. A.; Tute, M. S. *J. Mol. Struct.* **1987**, *158*, 69−78. (p) Khalil, S. M. *Z. Naturforsch.* **1985**, *40A*, 1278−82.

(18) (a) Adamo, C.; Lelj, F. *Chem. Phys. Lett.* **1994**, *223*, 54−60. (b) Barone, V.; Adamo, C. *J. Phys. Chem.* **1995**, *99*, 15062−8. (c) Hall, R. J.; Burton, N. A.; Hillier, I. H.; Young, P. E. *Chem. Phys. Lett.* **1994**, *220*, 129−132.

(19) (a) Takasuka, M.; Saito, T.; Nakai, H. *Vib. Spectrosc.* **1996**, *13*, 65−74. (b) Castillo, S.; Favrot, J.; Boussou, T.; Brazier, J. F.; Boisdon, M. T.; Zwick, A. *Spectrochim. Acta, Part A* **1994**, *50A*, 1121−1139. (c) Medhi, K. C. *Bull Chem. Soc. Jpn.* **1991**, *64*, 1944−50.

(20) Mukherjee, K. M.; Misra, T. N. *J. Raman Spectrosc.* **1996**, *27*, 595−600.

(21) Hatherley, L. D.; Brown, R. D.; Godfrey, P. D.; Pierlot, A. P.; Caminati, W.; Damiani, D.; Melandri, S.; Favero, L. B. *J. Phys. Chem.* **1993**, *97*, 46−51.

(22) (a) Held, A.; Champagne, B. B.; Pratt, D. W. *J. Chem. Phys.* **1991**, *95*, 8732−43. (b) Pratt, D. W. *NATO ASI Ser., Ser. C* **1996**, 483. (c) Borovikov, Yu. Ya.; Makovetskii, V. P.; Borovikova, G. S.; Nikolaenko, T. K.; Vovk, D. N. *Zh. Obshch. Khim.* **1994**, *64*, 2026−31; *Chem. Abstr.* **1998**, *123*, 32541.

(23) (a) Kuzuya, M.; Noguchi, A.; Okuda, T. *J. Chem. Soc., Perkin Trans. 2* **1985**, 1423−27. (b) Kuzuya, M.; Noguchi, A.; Okuda, T. *J. Chem. Soc., Chem. Commun.* **1984**, 435−38.

(24) (a) Ozeki, H.; Cockett, M. C. R.; Okuyama, K.; Takahashi, M.; Kimura, K. *J. Phys. Chem.* **1995**, *99*, 8608−8612. (b) Nimlos, M. R.; Kelley, D. F.; Bernstein, E. R. *J. Phys. Chem.* **1989**, *93*, 643−651. (c) Tembreull, R. S.; Chung, H.; Pang, H. M.; Lubman, D. M. *Anal. Chem.* **1985**, *57*, 2911−17.

(25) Baldwin, M. A.; Langley, G. J. *J. Chem. Soc., Perkin Trans. 2* **1988**, 347.

(26) (a) Naik, D. B.; Moorthy, P. N. *Proc. Indian Acad. Sci., Chem. Sci.* **1991**, *103*, 667−675; *Chem. Abstr.* **1991**, *116*, 20535. (b) Zatonskii, S. V.; Saraeva, V. V. *VINITI Deposited Doc.* **1984**, 3401; *Chem. Abstr.* **1984**, *103*, 64141.

(27) Ansari, M. A. *Indian J. Chem. Sect. B* **1985**, *24B*, 972−3.

(28) (a) Suishu, T.; Tsuru, S.; Shimo, T.; Somekawa, K.; *J. Heterocycl. Chem.* **1997**, *34*, 1005−1011. (b) Testa, A. C. *J. Photochem. Photobiol., A* **1992**, *64*, 73−77. (c) Somekawa, K.; Izumi, R.; Taniguchi, K.; Suishu, T.; Tokita, S. *Nippon Kagaku Kaishi* **1990**, 271−278.

(29) Turecek, F.; Gu, M.; Shaffer, S. A. *J. Am. Soc. Mass Spectrom.* **1992**, *3*, 493.

(30) (a) Danis, P.; Feng, R.; McLafferty, F. W. *Anal. Chem.* **1986**, *58*, 348. (b) Turecek, F.; Drinkwater, D. E.; Maquestiau, A.; McLafferty, F. W. *Org. Mass Spectrom.* **1989**, *24*, 669. (c) Shaffer, S. A.; Turecek, F.; Cerny, R. L. *J. Am. Chem. Soc.* **1994**, *115*, 12117.

(31) *Gaussian 94*, Revisions B.2 and E.1; Frisch, M. J.; Trucks, G. W.; Schlegel, H. B.; Gill, P. M. W.; Johnson, B. G.; Robb, M. A.; Cheeseman, J. R.; Keith, T. A.; Petersson, G. A.; Montgomery, J. A.; Raghavachari, K.; Al-Laham, M. A.; Zakrzewski, V. G.; Ortiz, J. V.; Foresman, J. B.; Cioslowski, J.; Stefanov, B. B.; Nanayakkara, A.; Challacombe, M.; Peng, C. Y.; Ayala, P. Y.; Chen, W.; Wong, M. W.; Andres, J. L.; Replogle, E. S.; Gomperts, R.; Martin, R. L.; Fox, D. J.; Binkley, J. S.; Defrees, D. J.; Baker, J.; Stewart, J. P.; Head-Gordon, M.; Gonzalez, C.; Pople, J. A. Gaussian, Inc.: Pittsburgh, PA, 1995.

(32) (a) Hehre, W. J.; Radom, L.; Schleyer, P. v. R.; Pople, J. A. *Ab Initio Molecular Orbital Theory*; Wiley: New York, 1986; pp 228−236. For other scaling factors, see: (b) Scott, A. P.; Radom, L. *J. Phys. Chem.* **1996**, *100*, 16502−16513.

(33) Møller, C.; Plesset, M. S. *Phys. Rev.* **1934**, *46*, 618.

(34) (a) Mayer, I. *Adv. Quantum Chem.* **1980**, *12*, 189. (b) Schlegel, H. B. *J. Chem. Phys.* **1986**, *84*, 4530.

(35) (a) Becke, A. D. *J. Chem. Phys.* **1993**, *98*, 1373 and 5648. (b) Stephens, P. J.; Devlin, F. J.; Chablowski, C. F.; Frisch, M. J. *J. Phys. Chem.* **1994**, *98*, 11623.

(36) Vosko, S. H.; Wilk, L.; Nusair, M. *Can. J. Phys.* **1980**, *58*, 120.

(37) Lee, C.; Yang, W.; Parr, R. G. *Phys. Rev. B* **1988**, *37*, 785.

(38) Turecek, F.; Wolken, J. K. *J. Am. Chem. Soc.*, **1999**. Submitted for publication.

(39) Pople, J. A.; Head-Gordon, M.; Raghavachari, K. *J. Chem. Phys.* **1987**, *87*, 5968−5975.

(40) (a) Zhu, L.; Hase, W. L. *Quantum Chemistry Program Exchange*; Indiana University: Bloomington, IN, 1994; Program No. QCPE 644. (b) Zhu, L.; Hase, W. L. *Chem. Phys. Lett.* **1990**, *175*, 117.

(41) Foresman, J. B.; Head-Gordon, M.; Pople, J. A.; Frisch, M. J. *J. Phys. Chem.* **1992**, *96*, 135−149.

(42) The proton affinities for the reagent gases were taken from Mallard, W. G.; Lindstrom, P. J., Eds.; *NIST Chemistry Webbook, NIST Standard Reference Database*; National Institute of Science and Technology, Gaithersburg, MD 1998; Vol. 69, http://webbook.nist.gov/chemistry.

(43) (a) Bohme, D. K.; Mackay, G. I.; Schiff, H. I. *J. Chem. Phys.* **1980**, *73*, 4976. For a review see (b) Harrison, A. G. *Chemical Ionization Mass Spectrometry*, 2nd ed.; CRC Press: Boca Raton, 1992; pp 17−18.

(44) Aue, D. H.; Webb, H. M.; Davidson, W. R.; Toure, P.; Hopkins, H. P., Jr.; Moulik, S. P.; Jahagirdar, D. V. *J. Am. Chem. Soc.* **1991**, *113*, 1770.

(45) Brown, R. S.; Tse, A.; Vederas, J. C. *J. Am. Chem. Soc.* **1980**, *102*, 1175−1176.

(46) Matyus, P.; Fuji, K.; Tanak, K. *Tetrahedron* **1994**, *50*, 2405−2414.

(47) (a) Dommrose, A.-F.; Grutzmacher, H.-F. *Int. J. Mass Spectrom. Ion Processes* **1987**, *76*, 95. (b) Dommrose, A.-F.; Grutzmacher, H.-F. *Org. Mass Spectrom.* **1987**, *22*, 437. (c) Wolf, R.; Dommrose, A.-F.; Grutzmacher, H.-F. *Org. Mass Spectrom.* **1988**, *23*, 26. (d) Wolf, R.; Grutzmacher, H.-F. *Org. Mass Spectrom.* **1989**, *24*, 398. (e) Surig, T.; Grutzmacher, H.-F. *Org. Mass Spectrom.* **1990**, *25*, 446.

(48) From the heats of formation (kJ mol^{-1}) of **1a** (−80), **1b** (−77), **1a**$^{+\bullet}$ (735), **1b**$^{+\bullet}$ (785), H$^{\bullet}$ (218), H^{+} (1530) and the proton affinities of **1a** (922) and **1b** (930).

(49) For a discussion of energy barriers to proton migrations in aromatic ions, see: (a) Mason, R.; Milton, D.; Harris, F. *J. Chem. Soc., Chem. Commun.* **1987**, 1453. (b) Hrusak, J.; Schroder, D.; Weiske, T.; Schwarz, H. *J. Am. Chem. Soc.* **1993**, *115*, 2015. (c) Glukhovtsev, M. N.; Pross, A.; Nicolaides, A.; Radom, L. *J. Chem. Soc., Chem. Commun.* **1995**, 2347. (d) Szulejko, J. E.; Hrusak, J.; McMahon, T. B. *J. Mass Spectrom.* **1997**, *32*, 494.

(50) Bush, K. L.; Glish, G. L.; McLuckey, S. A. *Mass Spectrometry/Mass Spectrometry*; VCH Publishers: New York: 1988; p 75.

(51) Baker, J.; Scheiner, A.; Andzelm, J. *Chem. Phys. Lett.* **1993**, *216*, 380−388.

(52) McMillen, D. F.; Golden, D. M. *Annu. Rev. Phys. Chem.* **1982**, *33*, 493−532.

(53) (a) Burkey, T. J.; Castelhano, A. L.; Griller, D.; Lossing, F. P. *J. Am. Chem. Soc.* **1983**, *105*, 4701−4703. (c) MacInnes, I.; Walton, J. C.; Nonhebel, D. C. *J. Chem. Soc., Perkin Trans. 2* **1987**, 1789−1793.

(54) Bordwell, F. G.; Zhang, X.-M.; Alnajjar, M. S. *J. Am. Chem. Soc.* **1992**, *114*, 7623−7629.

(55) Sustmann, R.; Korth, H.-G. *Adv. Phys. Org. Chem.* **1990**, *26*, 131−178.

(56) (a) Wiliams, B. W.; Porter, R. F.; *J. Chem. Phys.* **1980**, *73*, 5598. (b) Jeon, S.-J.; Raksit, A. B.; Gellene, G. I.; Porter, R. F. *J. Am. Chem. Soc.* **1985**, *107*, 4129. (c) Boldyrev, A. I.; Simons, J. *J. Chem. Phys.* **1992**, *97*, 6621. (d) Shaffer, S. A.; Turecek, F. *J. Am. Chem. Soc.* **1994**, *116*, 8647. (e) Shaffer, S. A.; Turecek, F. *J. Am. Soc. Mass Spectrom.* **1995**, *6*, 1004. (f) Shaffer, S. A.; Sadílek, M.; Turecek, F. *J. Org. Chem.* **1996**, *61*, 5234. (g) Nguyen, V. Q.; Sadilek, M.; Frank, A. J.; Ferrier, J. G.; Turecek, F. *J. Phys. Chem. A*, **1997**, *101*, 3789. (h) Wolken, J. K.; Nguyen, V. Q.; Turecek, F. *J. Mass Spectrom.* **1997**, *32*, 1162. (i) Shaffer, S. A.; Wolken, J. K.; Turecek, F. *J. Am. Soc. Mass Spectrom.* **1997**, *8*, 1111. (j) Frøsig, L.; Turecek, F. *J. Am. Soc. Mass Spectrom.* **1998**, *9*, 242.

(57) (a) Gerson, F.; Gleiter, R.; Moshuk, G.; Dreiding, A. S. *J. Am. Chem. Soc.* **1974**, *96*, 2342. For a review see (b) Russell, G. A. In *The Chemistry of Enones*; Patai, S., Rappoport, Z., Eds.; Wiley-Interscience: Chichester, 1989; Chapter 11, pp 472−512.

(58) Fitch, W. L.; Sauter, A. D. *Anal. Chem.* **1983**, *55*, 832.

(59) Uggerud, E. *Adv. Mass Spectrom.* **1995**, *13*, 53.

(60) Hartland, G. V.; Qin, D.; Dai, H.-L.; Chen, C. *J. Chem. Phys.* **1997**, *107*, 2890.

(61) Turro, N. J. *Modern Molecular Photochemistry*; University Science Books: Mill Valley, 1991; p 70.